applied sciences

MDPI

Article

Fragility Analysis of Transmission Towers Subjected to Downburst Winds

Chao Zhu [1], Qingshan Yang [1], Dahai Wang [2,*], Guoqing Huang [1] and Shuguo Liang [3]

[1] School of Civil Engineering, Chongqing University, Chongqing 400044, China; zhuchao@cqu.edu.cn (C.Z.); qshyang@bjtu.edu.cn (Q.Y.); ghuang1001@gmail.com (G.H.)
[2] School of Civil Engineering and Architecture, Wuhan University of Technology, Wuhan 430070, China
[3] School of Civil and Building Engineering, Wuhan University, Wuhan 430072, China; liangsg@public.wh.hb.cn
* Correspondence: wangdahai@whut.edu.cn

Abstract: A downburst is a typical local highly intensive wind all over the world, which is attributed to be the main cause of wind damage to transmission lines in inland areas worldwide. The collapse accidents of transmission towers under the downburst still occur every year. Therefore, it is of great significance to assess the safety of the transmission towers under downbursts. The motivation of the present study is to propose a fragility assessment method for transmission towers under the action of a downburst considering the uncertainty of wind-resistance capacity and the stochastic wind load effect. First, the downburst wind field of the transmission tower with different wind attack angles and different radial distances is simulated according to the mixed stochastic model. Then, random material characteristic samples are generated by the Latin hypercube sampling technique and applied to establish uncertain finite element models for transmission towers. Next, the static nonlinear buckling analysis is carried out by numerical methods to determine the ultimate capacity under the downburst wind load. The parameter analysis of different wind attack angles and radial distances between the downburst and the tower is conducted to determine the most unfavorable location of the maximum response. The failure mode of the transmission tower and the probabilities of the initial failure main members are summarized. Finally, the fragility curves of the transmission tower under the downburst and the atmospheric boundary layer (ABL) wind are compared. The results show that the maximum response is located at $R = 1.6D$. Most of the initial buckling members are located close to the first section of the tower. The fragility curves of the tower under the downburst are more dangerous than the ABL wind with the attack angle increasing from 0° to 90°. Furthermore, considering the probability model of intensity and direction of the downburst and based on the previous fragility analysis, the collapse probability of the transmission tower caused by the downburst is obtained. By probability analysis of the parameters, including layout conditions, different directions, and different wind speeds, it is found that the most favorable arrangement is 157.5°, and the most unfavorable arrangement is 112.5°.

Keywords: downburst; transmission towers; fragility; nonlinear buckling analysis; atmospheric boundary layer wind

Citation: Zhu, C.; Yang, Q.; Wang, D.; Huang, G.; Liang, S. Fragility Analysis of Transmission Towers Subjected to Downburst Winds. *Appl. Sci.* **2023**, *13*, 9167. https://doi.org/10.3390/app13169167

Academic Editors: José António Correia, Won-Hee Kang and Junho Chun

Received: 4 May 2023
Revised: 23 July 2023
Accepted: 3 August 2023
Published: 11 August 2023

1. Introduction

Transmission lines have a major role in electrical energy transmission. Disruptions in electrical power due to transmission line structural failures cause devastating economic and social losses. Transmission lines are particularly sensitive to wind load because of the common characteristics of high-rise towers and long-span structures, such as tower height, large span, and strong flexibility. According to a survey conducted in the United States, Australia, and South Africa, more than 80% of the wind-induced collapse accidents of transmission towers are mainly caused by downbursts. In 2005, 10 towers of 550 kV transmission tower in East China Power Grid collapsed under the action of downbursts.

Based on the investigation of transmission tower damage accidents in Ontario, Canada, in recent 15 years, almost all accidents have been caused by strong winds, especially downbursts. A downburst is a kind of small-scale local strong wind near the ground, which is very sudden and destructive [1]. The velocity profile of downbursts is evidently different from that of ABL winds [2–4]. Consequently, the failure characteristics caused by downbursts and ABL winds are obviously different [5]. Transmission towers are prone to damage, even collapse, when subjected to downbursts [6–9], as shown in Figure 1.

Figure 1. Collapses of transmission towers under downburst winds.

The fragility analysis of transmission towers under downbursts is of great significance to evaluating the existing transmission towers and optimizing the new ones. It can provide support for the disaster prevention and mitigation strategies of government departments, and it can also provide important data for risk management and transfer in the insurance industry. In addition, it also provides a reference for the design, maintenance, and retrofit of transmission towers.

Many published works only discuss the fragility analysis of transmission towers under ABL winds. Fu et al. (2019) presented a simplified model of a transmission line and conducted a fragility analysis considering the uncertainties of structural parameters and wind loads [10]. Cai et al. (2019) described a modeling framework to evaluate the fragility of transmission towers under extreme winds [11]. Fu et al. (2020) introduced the calculation method of wind and rain loads, conducted a fragility analysis of transmission towers, and proposed the critical collapse surface [12]. Tian et al. (2020) conducted a fragility analysis of the transmission tower-line system to assess the anti-collapse performance and explored the effect of the length of side spans and wind attack angles [13]. Ma et al. (2021) presented a component-based fragility modeling framework for transmission towers and demonstrated that it can effectively evaluate the transmission tower fragility curve [14]. Wang et al. (2021) proposed a quasi-static approach to assess the fragility of a transmission tower under wind loads [15]. Dikshit et al. (2023) presented a novel moment-matching technique for handling such uncertainties and estimating the structural fragility of a transmission tower system [16]. Although these efforts have been made, fewer studies have been conducted on the systematic analysis of the wind-induced fragility of transmission towers under the downburst considering wind speed and direction.

Currently, the collapse accidents of transmission towers under the downburst have attracted extensive attention from scholars at home and abroad. There are few studies on the fragility analysis of a transmission tower under a downburst. Savory et al. (2001) illustrated the model for the wind velocity time history of microburst events and the loading on the transmission tower [17]. Hoxey et al. (2003) investigated the characteristics of downbursts through the experiment and performed a finite element analysis of different transmission towers [18]. Chen et al. (2004) presented a deterministic-stochastic hybrid model of the downburst and conducted the wind-induced response of the slender structure in the time domain [19]. Chay et al. (2006) used a stochastic model of the downburst to

explore the quasi-static loading conditions and compared these loads to the ABL loads [20]. Shehata et al. (2007) evaluated the effect of various downburst parameters on the performance of transmission towers and compared the structural behavior under the downburst with the result of the ABL load [21]. Damatty et al. (2012) studied the progressive failure of two transmission line systems under downburst wind loading [22]. Yang et al. (2016) aimed to assess the capacity curve of a tower within the tower-line system under a downburst [23]. Wang et al. (2018) proposed a method of multi-scale failure analysis of transmission towers under downburst wind loading [24]. Zheng et al. (2022) investigated the progressive collapse mechanisms of a transmission tower-line system under downburst wind loading by fully coupled dynamic simulations [25]. Mara et al. (2016) assessed the capacity curve of a transmission tower under modeled downburst wind loading and compared it with that obtained for an ABL wind loading profile [26]. Damatty et al. (2018) conducted an extensive parametric study on a number of transmission line systems to evaluate their critical response to downburst loads [27]. Elawady et al. (2018) reported the first aeroelastic test for a multi-span transmission line under a simulated downburst [28]. Ibrahim et al. (2019) explored the dynamic effect of downburst loading on these longitudinal forces and examined the validity of using quasi-static analysis [29]. Fang et al. (2022) revealed the wind-induced vibration response characteristics of a transmission tower-line system under a downburst [30]. Zhong et al. (2022) conducted a dynamic stability analysis of the transmission tower-line system under a downburst [31]. Scholars at home and abroad have conducted a lot of research on the wind-induced response of transmission towers under the effects of downbursts. The research on the fragility analysis of transmission towers under the downburst is very limited.

In this paper, the wind-induced fragility analysis of three types of transmission towers under the effects of the downburst is analyzed. The main contents of this paper are as follows. The uncertainty of resistance and the randomness of wind load effect are considered, the fragility curves of the transmission tower under a downburst and ABL wind are compared, and the uncertain collapse of the transmission tower under a downburst is conducted to obtain the position and corresponding probabilities of the initial buckling members of the tower. Combined with the probability of wind speed and direction data of a region, the failure probability of a downburst attacking the transmission line causing the collapse of the transmission tower at different attack directions is calculated, and the optimal layout of transmission towers under a given wind field is studied.

2. Fragility Analysis Framework

The task of wind-induced fragility analysis of a transmission tower is to determine the conditional probability of the tower reaching a certain failure limit state under the case of a certain wind speed. This can be described by a fragility curve, which is associated with the wind load strength and the failure limit state. Generally, the abscissa of this curve is the wind speed while its ordinate is the probability of structural responses exceeding the specified failure limit state. As mentioned previously, the current wind-induced fragility analysis generally focuses on the synoptic wind. Nonetheless, insufficient attention has been paid to that under downburst winds. In this section, a fragility analysis framework of transmission towers under downburst winds will be presented. First, three important parts of this framework, including the uncertain structural model of transmission towers, the downburst wind load model, and the capacity curve of transmission towers, will be introduced separately. The fragility analysis framework of transmission towers under downburst winds is then presented in detail.

2.1. Uncertain Structural Model of Transmission Towers

It is well known that the deterministic model cannot be used to conduct an uncertainty analysis. In order to estimate the strength capacity and identify the failure modes of transmission towers more accurately, the uncertain collapse analysis and fragility analysis of transmission towers are required. An important task of these two kinds of analyses is to

establish the uncertain structural model of transmission towers. For a transmission tower, there are many probable uncertain variables. For example, the geometric dimensions, material properties, subjected loads, initial conditions, and boundary conditions [32]. Among these random variables, the material properties are an important factor that is required to be carefully considered. To describe the uncertainties of a structural model, a probability distribution of a random variable is generally prescribed. During this process, the selection of an appropriate probability distribution seems to be very important. After the probability distribution has been determined, the Latin hypercube sampling (LHS) technique can be used to generate the random sample of the uncertain model [33], which will be introduced in detail in Section 3. Latin hypercube sampling is a stratified sampling method, which allows to achieve the same results with fewer sampling times as with many random samples.

2.2. Downburst Wind Load Model

In this study, only the static downburst is considered. The location of the center of the downburst relative to the center of the tower is defined using the radial distance R and the angle θ. The wind speed of the downburst changes with the change in the radial distance, which is one of the main factors affecting wind speed. Due to the influence of the climate, terrain, and other factors, the direction of the incoming flow at each transmission tower location is random and unpredictable. It is essential to consider the effect of wind attack angle. Assume that the downburst touchdown occurs at a point whose horizontal radial distance and wind attack angle with the transmission tower are R and θ, respectively, as shown in Figure 2. In this case, the downburst wind field acting on the transmission tower can then be modeled as

$$U(z,t) = \overline{U}(z,t) + u(z,t) \tag{1}$$

where $U(z,t)$ is the wind speed at the height z of the transmission tower; $\overline{U}(z,t)$ is the time-varying mean wind speed; $u(z,t)$ is the corresponding fluctuating wind.

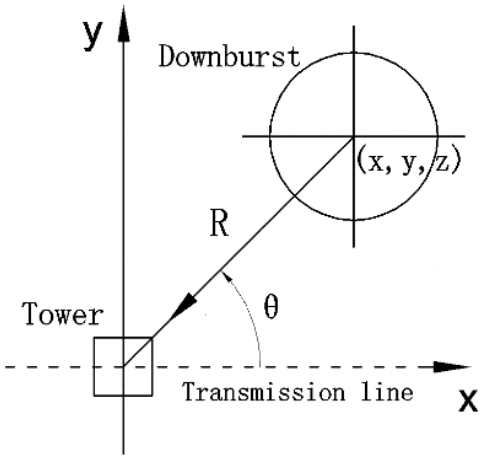

Figure 2. Relative position of transmission tower and downburst.

For the time-varying mean wind speed, it can be expressed as the product of a time-invariant vertical wind profile model and a time modulation function [19,34], i.e.,

$$\overline{U}(z,t) = \overline{U}(z)f(t) \tag{2}$$

where $\overline{U}(z)$ is the vertical wind profile; $f(t)$ is a modulation function whose maximum is one. This way of modeling the mean wind speed has an underlying assumption that the mean wind speeds reach their maximum values simultaneously.

Currently, there are many empirical models that have been used to describe the time-invariant mean wind profile of downburst winds [35,36]. In this study, the Vicroy wind profile model is chosen, which can be expressed as [37]

$$\overline{U}(z) = 1.22 \times \left[e^{-0.15z/z_{\max}} - e^{-3.2175z/z_{\max}}\right] \times V_{\max}(R) \tag{3}$$

where $z_{\max}$ denotes the height corresponding to the maximum horizontal wind speed; $V_{\max}(R)$ represents the maximum horizontal wind speed under the case of radial distance R, which can be given by

$$V_{\max}(R) = \begin{cases} V_{R,\max} \times (R/R_{\max}), & 0 \le R < R_{\max} \\ V_{R,\max} \times \exp\left\{-[(R - R_{\max})/R_r]^2\right\}, & R \ge R_{\max} \end{cases} \tag{4}$$

where $V_{R,\max}$ is the maximum wind speed at a certain height in the wind speed field; $R_{\max}$ is the horizontal distance between the maximum wind speed point and the downburst collision point; R_r is the radial length scale factor. For the modulation function, the following model is employed

$$f_{(t)} = \begin{cases} t/300, & 0 \le t \le 300 \\ \exp\left[-(t - 300)/1800\right], & t > 300 \end{cases} \tag{5}$$

For stationary downbursts, the time modulation function does not change with changes in the radial distance. For mobile downbursts, the time modulation function changes with the radial distance. Once the radial distance is prescribed, the time-varying mean wind profile of the downburst can be obtained.

When it comes to the fluctuating wind, it is generally modeled as a nonstationary random process, which is described by the time-varying spectrum. Currently, there are many different ways to define the time-varying spectrum of nonstationary random processes. Among them, the evolutionary spectrum is widely utilized due to its clear physical significance, which is also employed in this study. For simplicity, the extended Kaimal spectrum is used to describe the target evolutionary spectrum of fluctuating wind acting on the transmission tower. Assume that the nonuniform modulated evolutionary power spectral density function (EPSD) $S(z_j, \omega, t)$ of the point at the height z_j can be prescribed by

$$S(z_j, \omega, t) = \left|A(z_j, \omega, t)\right|^2 S(z_j, \omega) \tag{6}$$

where $A(z_j, \omega, t)$ and $S(z_j, \omega)$ are, respectively, the modulation function and the spectrum of the corresponding stationary process, which can be expressed as [38].

$$A(z_j, \omega, t) = \sqrt{\frac{\overline{U}(z_j, t)}{\overline{U}(z_j)} \left[\left(1 + 50\frac{\omega z_j}{2\pi \overline{U}(z_j)}\right) \Big/ \left(1 + 50\frac{\omega z_j}{2\pi \overline{U}(z_j, t)}\right)\right]^{5/3}} \tag{7}$$

$$S(z_j, \omega) = \frac{1}{2}\frac{200}{2\pi} u_*^2 \frac{z_j}{\overline{U}(z_j)} \frac{1}{\left(1 + 50\frac{\omega z_j}{2\pi \overline{U}(z_j)}\right)^{5/3}} \tag{8}$$

where ω is the circular frequency; $\overline{U}(z_j) = \frac{1}{T}\int_0^T \overline{U}(z_j, t)dt$ is the temporally average wind speed of the time-varying mean wind speed; $u_* = k \cdot \overline{U}(z_j) \cdot [\ln(z_j/z_0)]^{-1}$ is the friction velocity; z_0 is the roughness of the ground; k is the Von Karman constant. Apart from the auto EPSD, the cross EPSD between the points at the height of z_j and z_k can be given by

$$S(z_j, z_k, \omega, t) = A(z_j, \omega, t) A(z_k, \omega, t) \sqrt{S(z_j, \omega)} \sqrt{S(z_k, \omega)} \Gamma(\omega) \tag{9}$$

where $S(z_j, z_k, \omega, t)$ is the cross EPSD; $\Gamma(\omega)$ is the Davenport time-invariant coherence function model, which can be expressed as

$$\Gamma(\omega) = \exp\left\{-\frac{\omega}{2\pi}\frac{\sqrt{C_y^2(y_j - y_k)^2 + C_z^2(z_j - z_k)^2}}{\frac{1}{2}\left[\overline{U}(z_j) + \overline{U}(z_k)\right]}\right\} \tag{10}$$

where y_j and y_k, respectively, denote the coordinate of the spatial point along the transmission line; C_y and C_z are, respectively, the decay factor corresponding to the y and z direction. Given the spectral matrix of downburst winds, the spectral representation method can be used to generate the wind speed time history [39,40].

Once the wind speed time history has been determined, the wind load can be obtained according to quasi-steady assumptions and the Chinese specifications (DL/T 5154-2012) [41]. When the wind attack angle is zero degrees, the wind load of the transmission tower can be expressed as

$$W_{sb}(z,t) = 1/2C_{Db}\rho U^2(z,t)A_b \tag{11}$$

where $\rho = 1.225\,\mathrm{kg/m^3}$ is the air density; $C_{Db} = 2.5$ is the drag coefficient corresponding to a zero-degree wind attack angle; A_b is the structural projected area of windward corresponding to a zero-degree wind attack angle. Similarly, when the wind attack angle is 90 degrees, the wind load of the transmission tower can be expressed as

$$W_{sa}(z,t) = 1/2C_{Da}\rho U^2(z,t)A_a \tag{12}$$

where C_{Da} is the drag coefficient corresponding to a 90-degree wind attack angle; A_a is the structural projected area of windward corresponding to a 90-degree wind attack angle. For the results of other wind attack angles, the reader can be referred to as Table 1, which is used in this study.

Table 1. Wind load of the transmission tower.

Wind Attack Angle	Wind Load of the Tower Body	
	x	y
0°	0	$W_{sb}(z,t)$
45°	$0.424K[W_{sa}(z,t) + W_{sb}(z,t)]$	$0.424K[W_{sa}(z,t) + W_{sb}(z,t)]$
60°	$K[0.747W_{sa}(z,t) + 0.249W_{sb}(z,t)]$	$K[0.431W_{sa}(z,t) + 0.144W_{sb}(z,t)]$
90°	$W_{sa}(z,t)$	0

The wind load of transmission line is given below.

$$W_x = \alpha\mu_z\mu_{sc}w_0\beta_c d l_p sin^2\theta \tag{13}$$

where W_x represents the standard value of wind load perpendicular to the transmission line; α is the wind pressure nonuniformity coefficient; μ_z is the height variation coefficient of wind pressure; μ_{sc} is the shape coefficient on wind load of the transmission line; w_0 is basic wind pressure; β_c is the wind vibration coefficient of the transmission line; d is the outer diameter of the transmission line; l_p is the horizontal span of the tower; θ is the included angle between the direction of transmission line and the wind direction.

The wind load of insulator string is calculated by

$$W_I = \mu_z w_0 A_s \tag{14}$$

where W_I represents the standard value of the wind load of insulator string. A_s is the calculated value of the projected area of the windward component.

2.3. Capacity Curve of Structural Model

The purpose of buckling analysis is to obtain the critical load of the structure from a stable equilibrium state to an unstable equilibrium state. The two commonly used analysis methods are eigenvalue buckling analysis of ideal structures and nonlinear buckling analysis of defective structures.

Eigenvalue buckling analysis can be used to predict the theoretical yield strength of an ideal linear structure. The advantage of eigenvalue buckling analysis is to obtain the critical load and buckling shape of the structure without complex nonlinear analysis. It can provide reference load values for nonlinear buckling analysis. Here, the first-order eigenvalue of the structure is solved by the block Lanczos method, and its governing equation is:

$$([K_\beta] + \lambda[K_\sigma])\{\psi\} = 0 \tag{15}$$

where λ is the characteristic value, that is, the load factor in common sense; $[K_\beta]$ is the elastic stiffness matrix of the structure; $[K_\beta]$ is the reference initial stress matrix. $\{\psi\}$ is the characteristic displacement vector.

In order to consider the effect of initial geometric defects on the theoretical buckling strength of the structure, the nonlinear buckling analysis of the structure based on the large deflection finite element theory must be carried out. The cylindrical equal arc length method is widely used to track the nonlinear equilibrium route. In the iterative process, the load convergence criterion is selected as the criterion of convergence, i.e.,

$$\sqrt{\{g\}^T\{g\}} \le \beta\sqrt{\{q\}^T\{q\}} \tag{16}$$

where, $\{g\}$ is the unbalance node force vector; $\{q\}$ is the reference load vector; β is a parameter, which can be taken as 10^{-5}. If the number of iterations has exceeded a predetermined maximum or the displacement vector is becoming larger and larger, it is regarded as a divergence.

Transmission towers are often damaged due to instability. The accident investigation shows that many failures of transmission towers are caused by the buckling of compressed leg members or support members. This can be unveiled by analyzing its force-deformation curve or capacity curve. Nonlinear buckling analysis uses the static analysis method with gradually increasing load to determine the critical load that makes the structure unstable. This analysis method can consider the effects of geometric nonlinearity, material nonlinearity, and initial defects at the same time.

By analyzing the relationship between the component failure and overall failure, this paper reveals the whole process of transmission tower failure under the action of a downburst so as to establish a reasonable failure criterion to classify the failure level of transmission towers.

Nonlinear buckling analysis is performed on the transmission tower to obtain the top displacement base shear bearing capacity curve. At the same time, the maximum Mises stress of all main and diagonal components of the transmission tower can be extracted at each step of the loading process to obtain the top displacement main material maximum Mises stress curve and the top displacement diagonal material maximum Mises stress curve. The three curves are drawn and analyzed simultaneously. For different tower types and due to structural reasons, there are two situations: the first is that the main material yields before the diagonal material, as shown in Figure 3a; the second is that the diagonal material yields before the main material, as shown in Figure 3b.

When the main material yields before the diagonal material, it can be observed that as the wind load continues to increase, when the top displacement of the tower reaches X_I, the maximum stress of the main material reaches the yield strength before the diagonal material. As the main load-bearing component of the transmission tower is the main material, the overall structure of the tower begins to enter nonlinearity. When the displacement of the tower top reaches X_{II}, the diagonal material near the maximum stress of the main material

reaches its yield strength. When the displacement of the tower top reaches X_{III}, the overall wind load and base shear force reach their peak. The three curves under different directional angles have the same variation characteristics. Based on the above analysis, when the main material of the transmission tower reaches the yield strength, it can be defined that the structure undergoes slight damage. When both the main and diagonal materials of the transmission tower reach yield, the structure undergoes severe damage. When the overall wind load of the transmission tower reaches its peak, the structure collapses and fails.

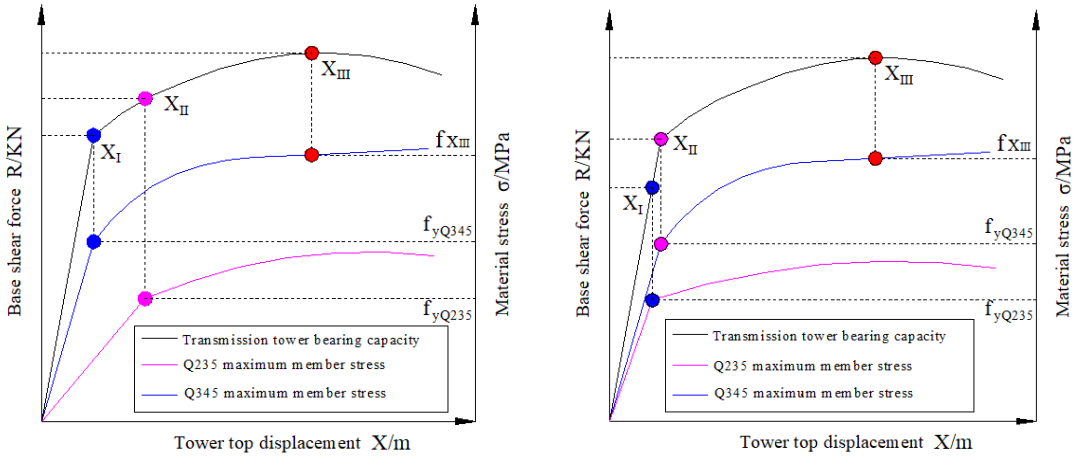

(**a**) The main material yields first (**b**) The diagonal material yields first

Figure 3. Failure criteria.

When the diagonal material yields before the main material, it can be observed that as the wind load continues to increase, when the top displacement of the tower reaches X_I, the maximum stress of the diagonal material reaches its yield strength before the main material. As loading continues, when the top displacement of the tower reaches X_{II}, the maximum stress of the main material reaches the yield strength, and the overall structure of the tower begins to enter nonlinearity. When the displacement of the tower top reaches X_{III}, the wind load and base shear force reach their peak. The three curves under different directional angles have the same variation characteristics. Based on the above analysis, when the diagonal material of the transmission tower reaches the yield strength, it can be defined that the structure undergoes slight damage. When both the main and diagonal materials of the transmission tower reach yield, the structure undergoes severe damage. When the overall wind load of the transmission tower reaches its peak, the structure collapses and fails.

2.4. Proposed Fragility Analysis Framework

Through the wind-induced fragility analysis of transmission towers under downburst, the possibility of reaching the limit state can be obtained under different wind speeds in all directions; the relationship between the wind load strength and the damage degree of the tower is determined, and the wind resistance of the tower is quantitatively calculated in the way of probability. In this paper, the horizontal tower top displacement is selected as the structural performance index, the structural collapse limit state is divided, and the wind-induced fragility is studied. The procedure of fragility analysis of the transmission towers under downburst is described in Figure 4.

The basic steps and flow chart are as follows:

(1) Considering the uncertainty of the transmission tower, the Latin hypercube sampling method is used to simulate 20 random structure samples [33], denoted by S_i, $i = 1, 2, \cdots, 20$;

(2) Considering the randomness of wind load, the downburst wind field with different direction angles and radial distances is simulated based on the hybrid random theory and converted into the wind load according to the specifications.
(3) The nonlinear buckling analysis is carried out for each structure sample S_i to determine the threshold displacement values of the collapse of the structure Δ_{c_i}, $i = 1, 2, \cdots, 20$;
(4) The wind-induced response of each uncertain structural sample S_i under different radial distances and direction angles is analyzed. Tower top displacement at different radial distances of the transmission tower is calculated. As the wind-induced response of the transmission tower increases first and then decreases with the increase in the radial distance, the radial distance (R_{a_i}, R_{b_i} $i = 1, 2, \cdots, 20$) between the maximum tower top displacement exceeding Δ_{c_i} for the first time and the last time can be obtained. At the same time, the average wind speed (V_{ai}, V_{bi}, $i = 1, 2, \cdots, 20$) is recorded at the 10 m height of the tower at the corresponding position. Thus, the curve of radial distance vs. failure probability of the collapse state of the tower can be drawn.
(5) By comparison, the average wind speed ($V_i = Min(V_{a_i}, V_{b_i})$ $i = 1, 2, \cdots, 20$) at 10 m height when the transmission tower collapses can be obtained, and then the fragility curve of the collapsed state of the tower for a wind attack angle can be drawn.
(6) Using the above method, the fragility curves of slight damage and severe damage of the transmission tower can also be obtained.

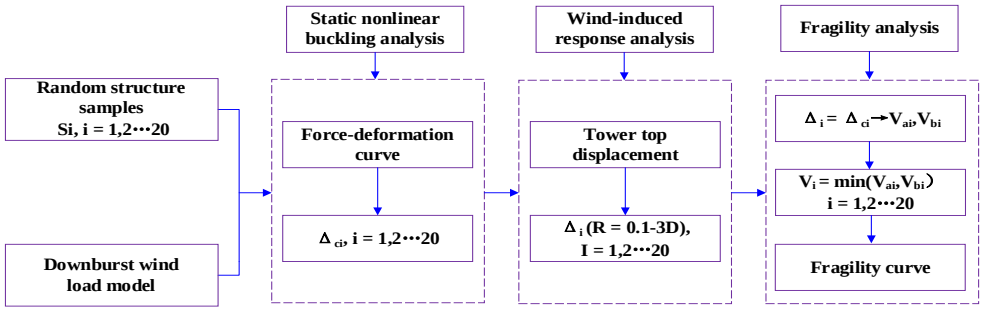

Figure 4. Flow chart of the proposed fragility analysis framework.

3. Typical Engineering Case Study

In this section, a fragility analysis of three typical prototypes of transmission towers is conducted to demonstrate the effectiveness of the proposed fragility analysis framework. Six parts, including the uncertain finite element model, downburst wind load, nonlinear buckling analysis, uncertain collapse analysis result, fragility analysis result, and failure probability analysis, will be presented in sequence.

3.1. Uncertain Finite Element Model

The 110 KV, 220 KV, and 35 KV linear transmission towers were selected as the research objects, with tower heights of 25 m, 28.2 m, and 33.9 m, respectively. The conductor of the 110 KV transmission tower was LGJ-400/35, and the ground wire was GJ-50. The conductor of the 220 KV transmission tower was LGJX-400/50, and the ground wire was GJ-50. The 35 KV transmission tower conductor was JL/LB20A-240/40, and the ground wire was GJ-55. The spans were 178 m, 339 m, and 320 m, respectively. The main material of the transmission tower was Q345-type angle steel, while the others were Q235-type angle steel. The three-dimensional finite element model of the transmission tower established using ANSYS software is shown in Figures 5–7. During the analysis, the ideal elastoplastic assumption was employed to consider the material nonlinearity. In addition, the yield strength criterion of the material followed the Von Mises criterion, and the bilinear kinematic hardening rule was used to model the constitutive model of the steel material.

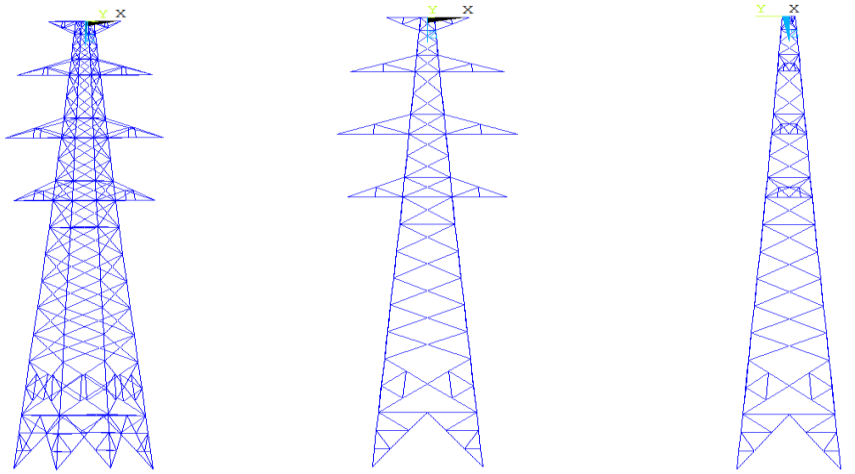

(**a**) Axonometric view (**b**) Front view (**c**) Side view

Figure 5. Finite element model of the 110 kV transmission tower.

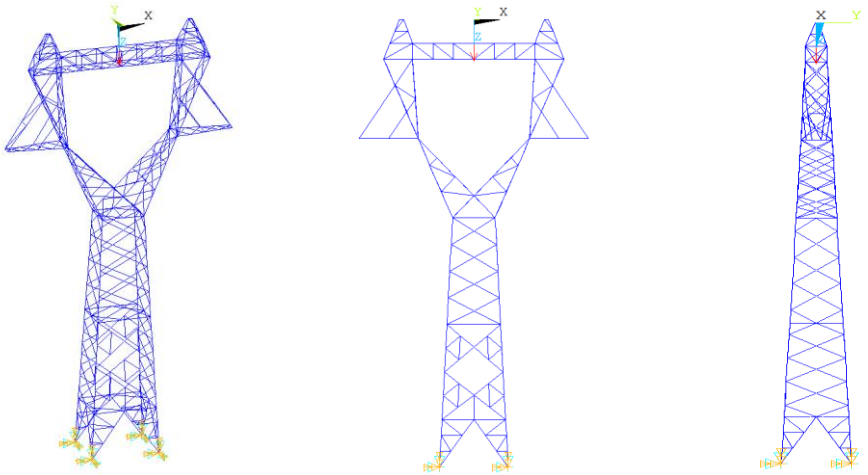

(**a**) Axonometric view (**b**) Front view (**c**) Side view

Figure 6. Finite element model of the 220 kV transmission tower.

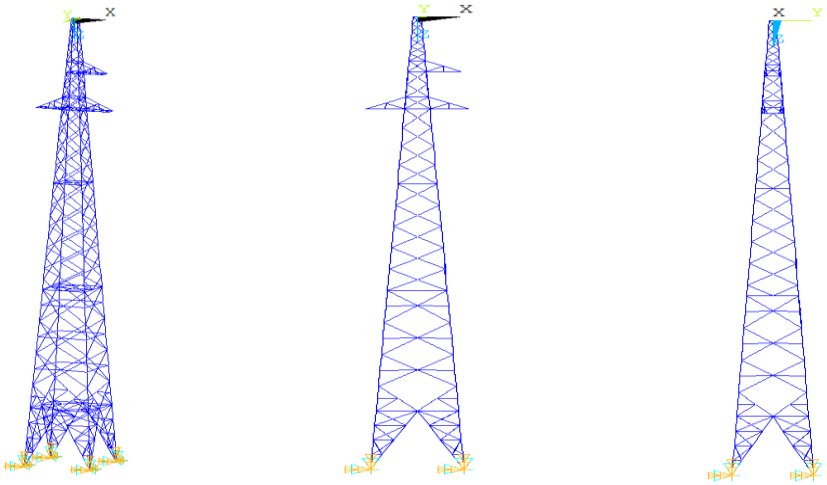

(**a**) Axonometric view (**b**) Front view (**c**) Side view

Figure 7. Finite element model of the 35 kV transmission tower.

Aboshosha et al. (2015) and Lei et al. (2018) compared the decoupling and coupling approaches through the numerical simulation analysis of dynamic response and found that tower line decoupling analysis can obtain good calculation accuracy and greatly reduce the time domain calculation time of wind vibration response of tower-line coupling system structures [42,43]. In this paper, the tower-line decoupling analysis is considered. Figure 8 shows the finite element model of conductor/ground wire. Table 2 shows the mechanical parameters of the cable of the 220 KV transmission tower. The insulator is the component that connects these cables to the transmission tower. The conductor insulator and the ground wire insulator are used, and their length is 4.5 m. The mechanical parameters of the insulator are given in Table 3. The link10 element is used for the conductor and insulator. The time history analysis is conducted according to the model in Figure 8, and the reaction force at the end of the insulator is extracted and will be exerted on the tower as a concentrated load.

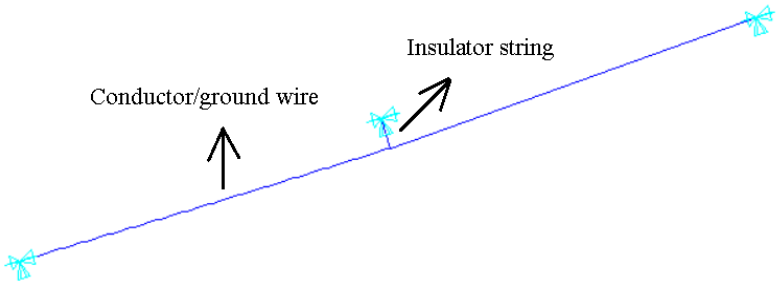

Figure 8. Finite element model of conductor/ground wire.

Table 2. The mechanical parameters of conductors and ground wires.

Material Properties	Conductors (LGJX-400/50)	Ground Wires (GJ-50)
Cross-sectional area	3.68×10^{-4} m^2	0.495×10^{-4} m^2
Initial tension	123,400 N	32,993 N
Elastic modulus	6.9×10^{10} Pa	1.85×10^{11} Pa
Line expansion coefficient	1.930×10^{-5} °C	1.15×10^{-5} °C
Density	3.35×10^{3} kg/m^3	7.96×10^{3} kg/m^3

Table 3. The mechanical parameters of insulators.

Material Properties	Insulator of Conductors	Insulator of Ground Wires
Cross-sectional area	0.1018 m^2	0.0452 m^2
Elastic modulus	7.8×10^{10} Pa	7.2×10^{10} Pa
Length	6.832 m	6.832 m
Density	1780.4 kg/m^3	1700 kg/m^3

As mentioned previously, the material properties are an important factor that requires comprehensive consideration. The main material property parameters of steel include density, Poisson's ratio, elastic modulus, yield strength, and so on. Table 4 lists the parameter values considered in the uncertainty analysis and their corresponding probability distribution. After that, the Latin hypercube sampling method is used to simulate the random variables, and the generated random samples are used to establish the structural uncertainty finite element model. This paper considers the influence of the uncertainty of density, Poisson's ratio, elastic modulus, and yield strength on vulnerability. Note that in tables, COV denotes the coefficient of variation. Figures 9 and 10 plot the generated random samples and indicate that the generated results are consistent with the target distribution type.

Table 4. Statistical information of material variables.

Uncertainty Source	Random Variable	Average Value	COV	Distribution Type
Elastic modulus	E_S	206 Gpa	0.03	Lognormal
Poisson ratio	v	0.3	0.03	Lognormal
Density	ρ	7800 kg/m^3	—	Deterministic
Yield strength for Q235	f_{y_Q235}	263.7 Mpa	0.07	Lognormal
Yield strength for Q345	f_{y_Q345}	387.1 Mpa	0.07	Lognormal

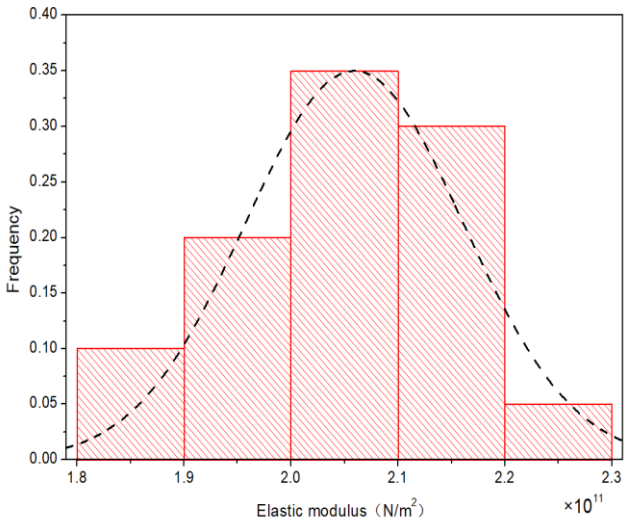

Figure 9. Generated samples of elastic modulus.

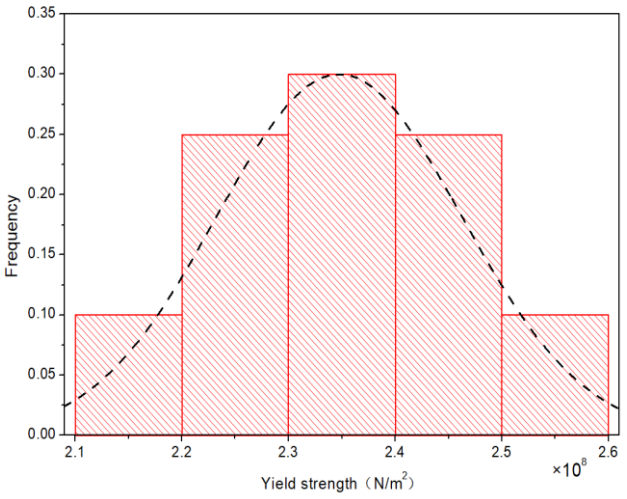

Figure 10. Generated samples of yield strength.

3.2. Downburst Wind Load Simulation

In this study, the downburst wind field with different combinations of direction angles and radial distances is addressed. Among them, four direction angles, including 0°, 45°, 60°, and 90°, are considered while the radial distances R range from 0.1D to 3D with an interval of 0.1D, where D = 600 m. Apart from the direction angles and radial distances, the other parameters related to the mean wind speed and fluctuation are summarized in Table 5. Note that the horizontal maximum wind speed associated with the Vicroy wind speed profile model is a result of a 3 s time interval. In order to be consistent with Chinese specifications of transmission line design in the practical application (DL/T 5154-2012), the 3 s mean wind speed will be converted to a 10 min mean wind speed according to the

converted formula [44]. The results are shown in Table 6. For the fluctuation, the tower is divided into six sections along the height when simulating the downburst wind field, as shown in Table 6. Hence, a total of six points are required to be simulated. The ensemble autocorrelation function of one point and the cross-correlation function between two points estimated from 2000 samples are shown in Figure 11. It can be seen that they agree with the targets well, which verifies the simulation accuracy of the downburst fluctuating winds. Once the time history of the downburst wind field has been generated, the time histories of wind force can be calculated based on Equations (11)–(14) and Table 1. The wind-induced response of the transmission tower can then be conduced.

Table 5. The main parameters used in the simulation of the downburst wind field.

Parameter	Mean Wind Speed					Fluctuating Wind			
	Z_{max}	V_{max}	$V_{R,max}$	R_{max}	R_r	Z_0	k	C_y	C_z
Value	70 m	80 m/s	47 m/s	1000 m	700 m	0.00127	0.4	14	10

Table 6. Wind velocity at the centroid points of each wind pressure section.

Point Number	z/m	$\overline{U}_3(z)$ (m/s)	$\overline{U}(z)$ (m/s)
1	5	19.0	13.4
2	10	33.9	23.8
3	15	45.5	32.0
4	20	54.6	38.4
5	25	61.6	43.3
6	28.2	64.9	45.7

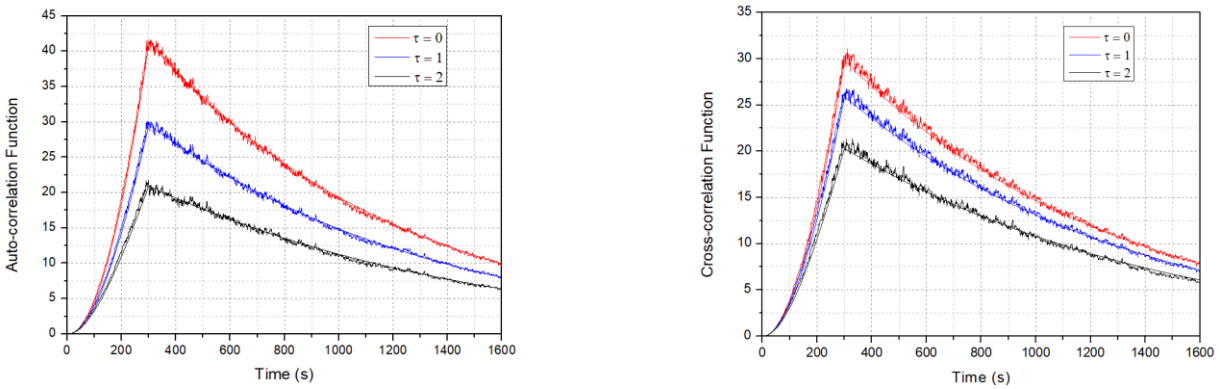

(**a**) Autocorrelation function (**b**) Cross-correlation function

Figure 11. Comparison of estimated auto-/cross correlation with targets (2000 samples).

3.3. Nonlinear Buckling Analysis

As mentioned previously, the nonlinear buckling analysis of the transmission tower under a downburst is conducted by finite element analysis. First, the eigenvalue buckling analysis of the transmission tower structure is carried out. According to the results of the eigenvalue buckling analysis, the initial defects are imposed by the deformation of the eigenvalue buckling mode. The nonlinear buckling analysis of the transmission tower is then carried out, and the force-deformation curves of the top displacement of transmission towers under different wind attack angles are obtained, as shown in Figure 12. It can be found that 45° and 60° directional angles are more prone to buckling failure, and 0° and 90° directional angles have better ductility. The threshold displacement values of different damage states of transmission towers can be obtained. Subsequently, the uncertain collapse analysis result and fragility analysis result can be obtained.

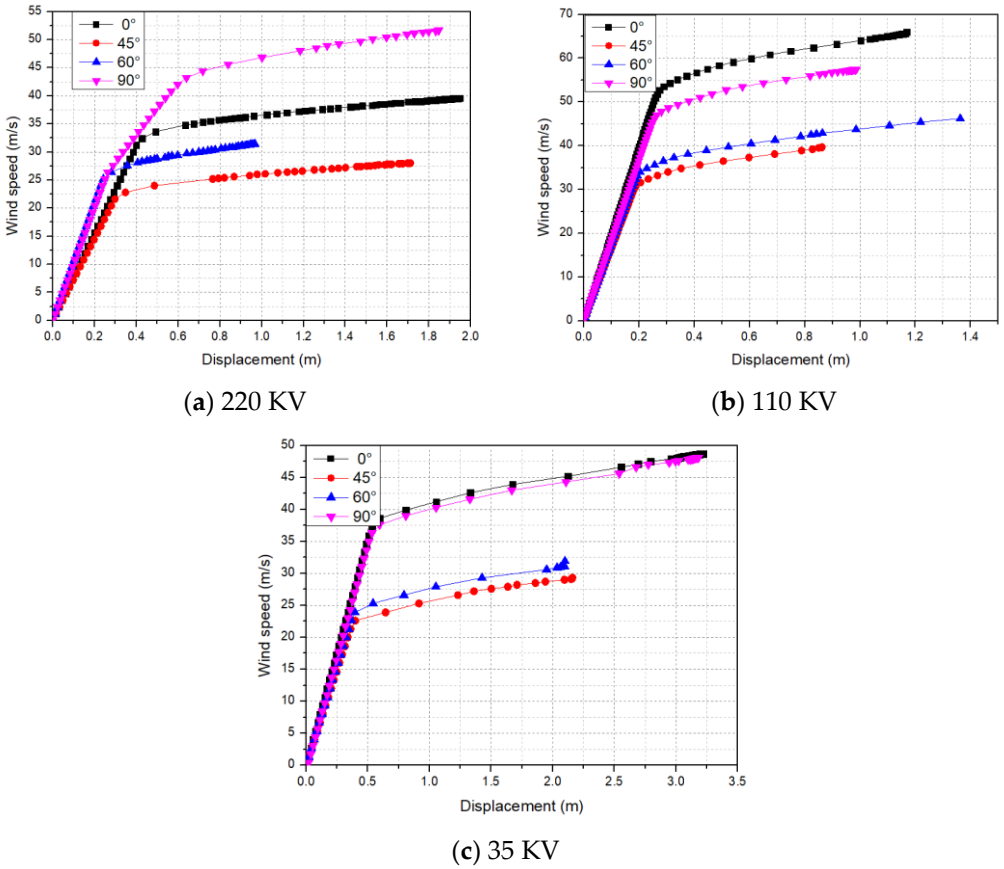

(**a**) 220 KV (**b**) 110 KV

(**c**) 35 KV

Figure 12. Capacity curve of one structural sample under different wind attack angles.

3.4. Uncertain Nonlinear Capacity Behavior Analysis

Based on whether to consider the uncertainties of the structural model, the collapse analysis can be divided into two categories: i.e., the uncertain collapse analysis and deterministic collapse analysis. The latter cannot fully consider the influence of the uncertainty of the selected parameters on the performance of the tower. On the contrary, the uncertain collapse analysis can completely evaluate the collapse state of the transmission tower under the downburst. In addition, the wind attack angle is also an important influence factor on the collapse result. The influence of different wind attack angles on the initial failure members requires deep investigation.

In this study, both the deterministic collapse analysis and uncertain collapse analysis of the 220 KV transmission tower under different cases of wind attack angles are carried out through the nonlinear buckling analysis method. For the uncertain collapse analysis, the parameters of the uncertain structural model introduced in Section 3.1 will be employed, where 20 samples are generated. Figures 13–15 include the stress nephogram of initial buckling state at 0° direction angle, the position, and the corresponding probability of the initial buckling member at each direction angle of the deterministic model and uncertain model. In the figure, "0°, 100%" indicates that the failure probability of the corresponding member at the 0° direction angle is 100%. It can be found that most of the initial buckling members are located near the first section of the transmission tower. The initial failure member is the main member, indicating that the main failure mode of the transmission tower belongs to bending failure. The main member is a compression bending component, which is the main component of the wind resistance of the transmission tower, while the diagonal member is an axial compression component, which is an auxiliary component of the wind resistance of the transmission tower. The instability of the diagonal member will not cause the collapse of the tower structure—it will only accelerate the instability of the main member. Considering the structural uncertainty is helpful to comprehensively

analyze the failure path of transmission towers. Therefore, uncertain collapse analysis is particularly important to determine the location and probability of all potential buckling failure members.

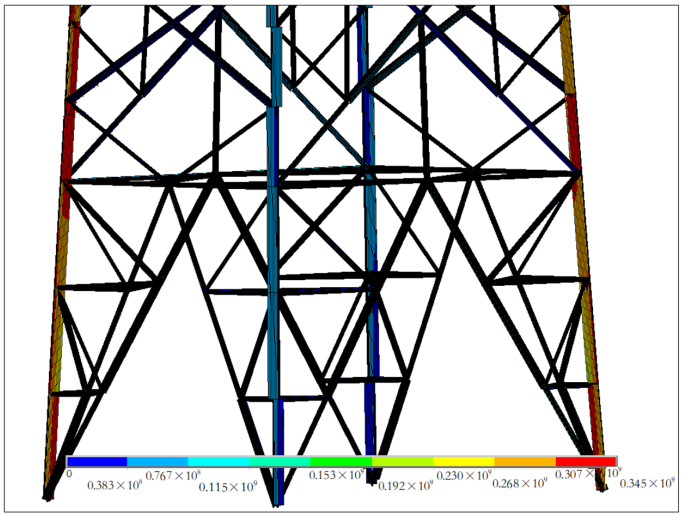

Figure 13. Stress nephogram of initial buckling state at 0° direction angle.

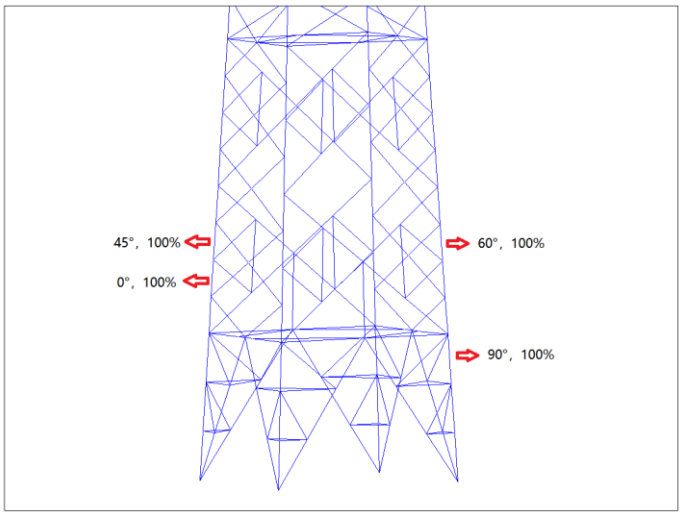

Figure 14. Initial buckling member position and corresponding probability at each direction angle of the deterministic model.

3.5. Fragility Analysis

3.5.1. Downburst Wind Load Case

In this paper, the wind-induced response of the transmission tower is carried out by simulating the downburst wind field with different direction angles and different radial distances ($R = 0.1D - 3D, \Delta R = 0.1D, D = 600$ m). The tower top displacement under the downburst at each direction angle first increases and then decreases with the increase in radial distance. Compared with the nonlinear buckling analysis results for each direction angle, the radial distance between the maximum tower top displacement at different direction angles exceeding the threshold displacement values of different damage states for the first time and the last time can be obtained. The radial distance when different damage states occur at different angles is shown in Tables 7–9, and the curve of radial distance vs. failure probability for different damage states of the 220 KV transmission tower at different wind angles can be obtained, as shown in Figure 16. It can be found that the location where the maximum response occurs is $R = 1.6D$, and the range of radial distance for slight

damage status is wider than that for severe damage at all direction angles—the range far greater than the radial distance of collapse. The reason is that the wind-induced response of the transmission tower under the downburst is the same as the mean wind speed of the downburst, which increases first and then decreases with the increase in the radial distance. After severe damage occurs to the transmission tower, only a small amount of load needs to be added to generate significant displacement, thus reaching a collapsed state. Therefore, the radial distance between the occurrence of severe damage and the collapse is relatively close, and the distance from slight damage is relatively far.

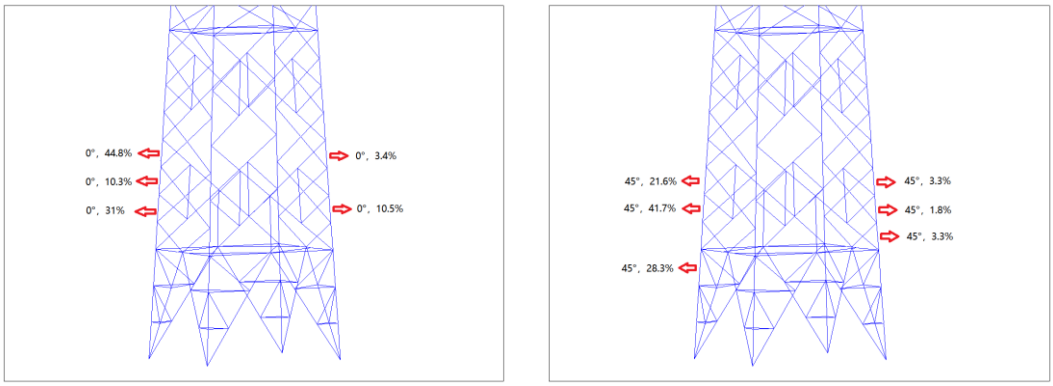

(**a**) 0° direction angle (**b**) 45° direction angle

(**c**) 60° direction angle (**d**) 90° direction angle

Figure 15. Initial buckling member position and corresponding probability at different direction angles of uncertain model.

Table 7. Dimensionless radial distance (R/D) with different angles in different damage states (220 KV).

Damage States	Wind Attack Angle			
	0°	**45°**	**60°**	**90°**
Slight damage	0.7~2.4	1.0~2.4	0.9~2.6	1.0~2.1
Severe damage	0.9~2.2	1.3~2.2	1.2~2.4	1.3~1.8
Collapse	1.0~2.1	1.4~2.1	1.3~2.3	1.4~1.7
Critical radial distance	1.6	1.6	1.6	1.6

Table 8. Dimensionless radial distance (R/D) with different angles in different damage states (110 KV).

Damage States	Wind Attack Angle			
	0°	**45°**	**60°**	**90°**
Slight damage	1.0~2.2	1.2~2.2	1.2~2.3	1.2~2.0
Severe damage	1.2~1.9	1.4~2.0	1.4~2.1	1.4~1.8
Collapse	1.3~1.8	1.5~1.9	1.5~2.0	1.5~1.7
Critical radial distance	1.6	1.6	1.6	1.6

Table 9. Dimensionless radial distance (R/D) with different angles in different damage states (35 KV).

Damage States	Wind Attack Angle			
	0°	**45°**	**60°**	**90°**
Slight damage	0.8~2.3	0.6~2.6	0.8~2.8	0.9~2.2
Severe damage	1.0~2.1	0.9~2.4	1.0~2.6	1.1~2.0
Collapse	1.1~2.0	1.0~2.3	1.1~2.5	1.2~1.9
Critical radial distance	1.6	1.6	1.6	1.6

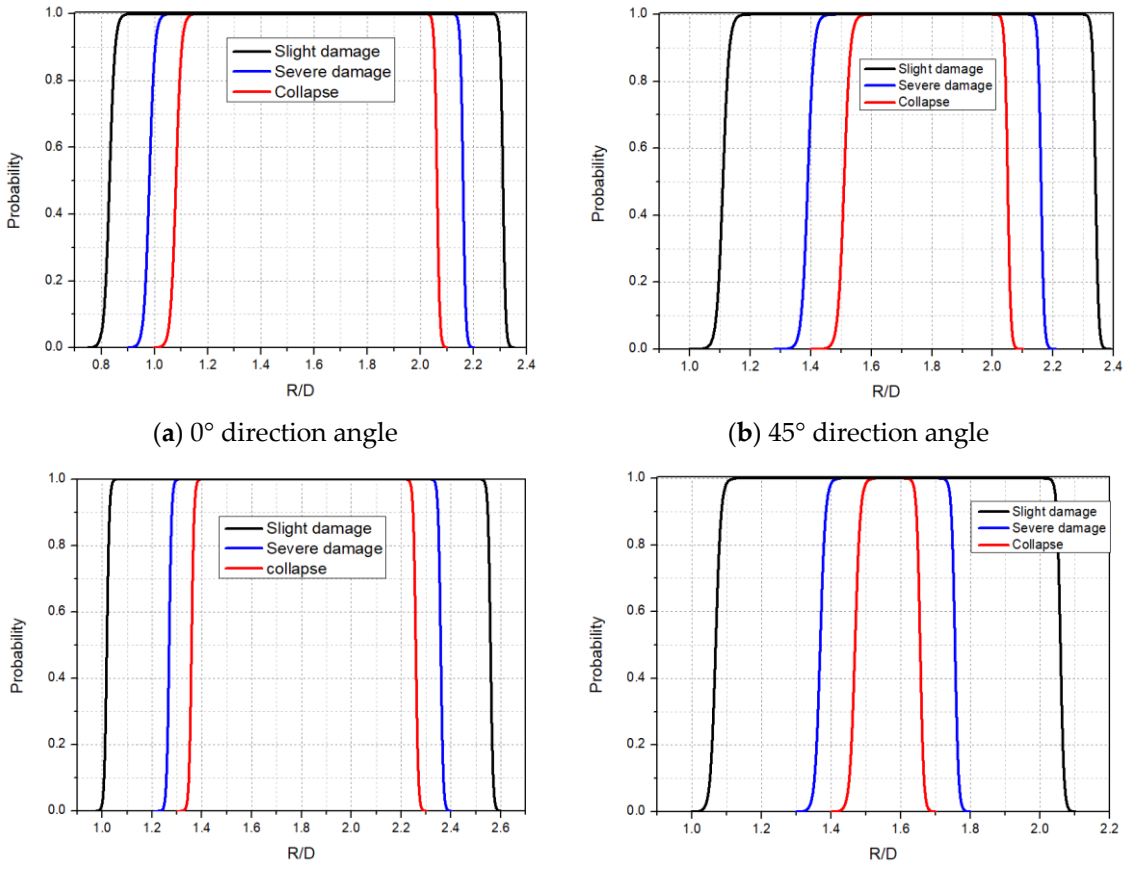

(**a**) 0° direction angle (**b**) 45° direction angle

(**c**) 60° direction angle (**d**) 90° direction angle

Figure 16. The curve of radial distance vs. failure probability for different damage states of the transmission tower at different wind angles.

In this paper, a total of 120 load cases are analyzed, considering 4 wind attack angles and 30 radial distances. For each case, 20 structural samples are applied in the nonlinear

finite element analysis, and each numerical analysis is much more time-consuming. To reduce the time consumption, the Latin hypercube sampling method, a kind of stratified sampling method, is adopted in this paper. The samples extracted from the high-dimension random space by this method are relatively uniform and do not produce obvious clustering phenomena. Compared with Monte Carlo sampling, the method of Latin hypercube sampling can achieve the same results using fewer samples. The probability of the capacity of the samples of the tower under the downburst is fitted by a lognormal distribution.

3.5.2. Comparison between ABL Wind and Downburst Wind

According to the above basic steps of fragility analysis of the transmission tower under the downburst, fragility curves in different directions can be obtained. At the same time, fragility curves under the ABL wind are carried out to compare and analyze the similarities and differences between them.

The basic steps of fragility analysis under the ABL wind are given as follows:

1. Considering the uncertainty of the transmission tower, the Latin hypercube sampling method is used to simulate 20 random structure samples, denoted by S_i, $i = 1, 2, \cdots, 20$;

2. The nonlinear buckling analysis is conducted for each structure sample S_i to determine the threshold displacement values of the collapse of the structure Δ_{c_i};

3. Incremental dynamic analysis (IDA) is carried out for a structure sample S_i under different basic wind speeds (v = 30–75 m/s, the increment is 0.1 m/s) to obtain the curve of maximum tower top displacement vs. basic wind speed, and the wind speed corresponding to the threshold displacement value of collapse can be found. They are denoted as v_{c_i}.

4. Considering the uncertainty of the transmission tower and the randomness of fluctuating components under the same basic wind speed, a total of 20 curves of maximum displacement vs. basic wind speed can be obtained. A total of 20 sets of Δ_{c_i} and v_{c_i} ($i = 1, 2, \cdots, 20$) can be determined.

5. From these values for v_{c_i}, the wind-induced fragility curves of the transmission tower can be drawn for a wind attack angle.

The above method is used for fragility analysis under the ABL wind. Wind fluctuations can be treated as the stationary Gaussian process and could be simulated using the spectral representation method [45,46]. Kaimal spectrum is used for the longitudinal wind fluctuation component. The terrain is set as category B and the profile exponent is 0.16. According to quasi-steady assumptions and the Chinese code (DL/T 5154-2012), the wind speed can be converted into wind load.

The transmission tower is a typical wind-sensitive structure. Because almost half of the wind load on the tower comes from large-span transmission lines, the wind load effect on the tower varies significantly in different wind directions. On the other hand, the ultimate wind resistance capacity of the tower is also different from the wind attack angle [47–49]. Both of these reasons lead to the significant variation in the fragility curves at different angles. Therefore, it is essential to study the influence of the wind attack angle on the fragility curves.

The fragility curves of the 220 KV transmission tower under the ABL wind and downburst are shown in Figures 17–20. Through comparison, it is found that with the increase in a wind direction angle, the critical collapse wind speed of the tower increases; the most unfavorable direction angle is 0°, and the most favorable direction angle is 90°. The critical collapse wind speed at each direction angle of the transmission tower under the downburst is significantly less than that under the ABL wind, and the larger the direction angle is, the greater the difference in critical collapse wind speed is. Similarly, the fragility curve of 110 KV and 35 KV transmission towers under the ABL wind is compared with the fragility curve of the collapse state under the downburst, as shown in Figures 21–24. The fragility curves of the tower under the downburst are more dangerous than the curves under the ABL wind with the attack angle increasing from 0° to 90°.

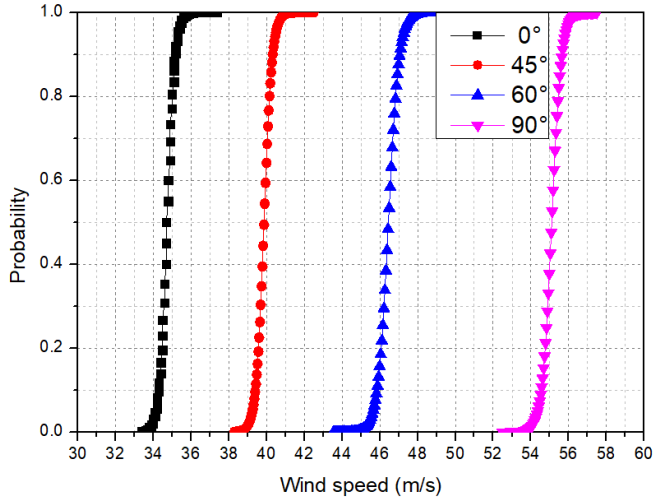

Figure 17. Fragility curve of collapse state of 220 KV transmission tower under ABL wind.

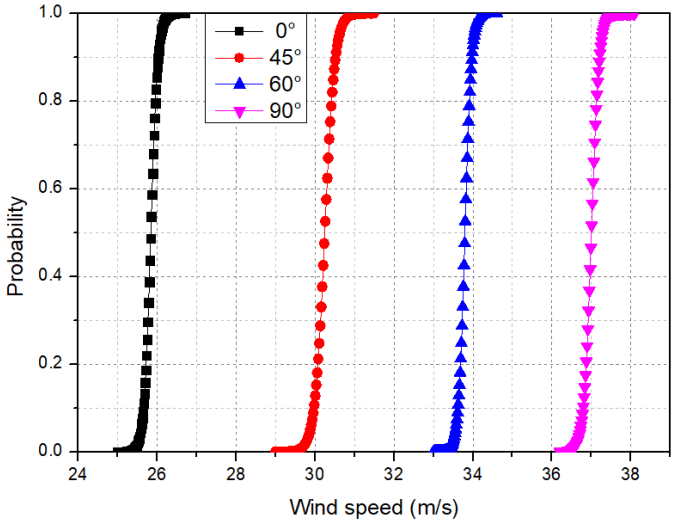

Figure 18. Fragility curve of slightly damaged state under downburst.

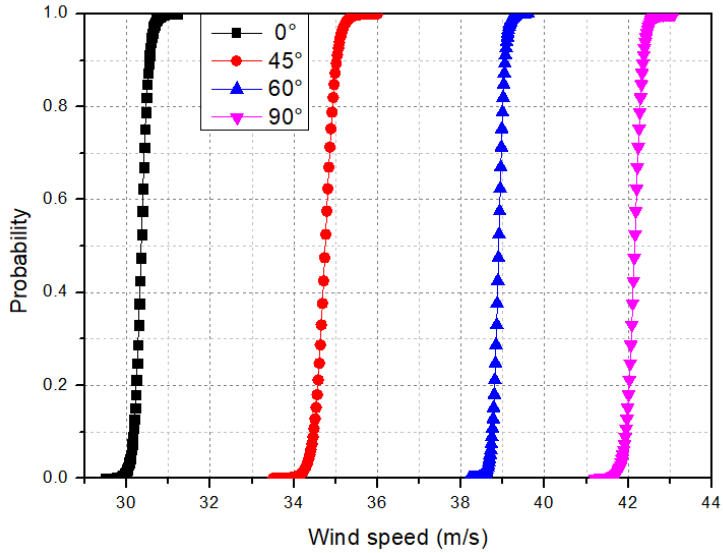

Figure 19. Fragility curve of severely damaged state under downburst.

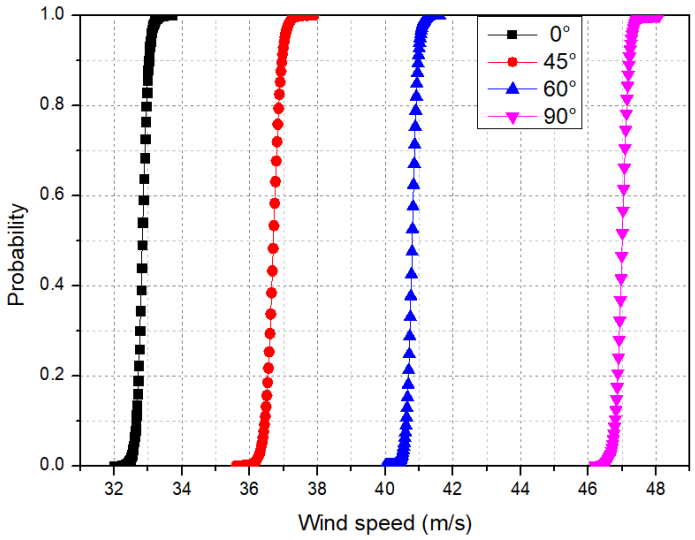

Figure 20. Fragility curve of collapse state under downburst.

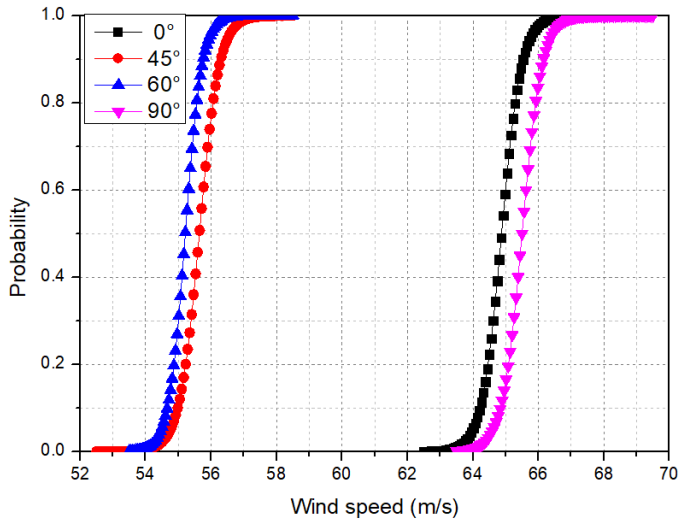

Figure 21. Fragility curve of collapse state of 110 KV transmission tower under ABL wind.

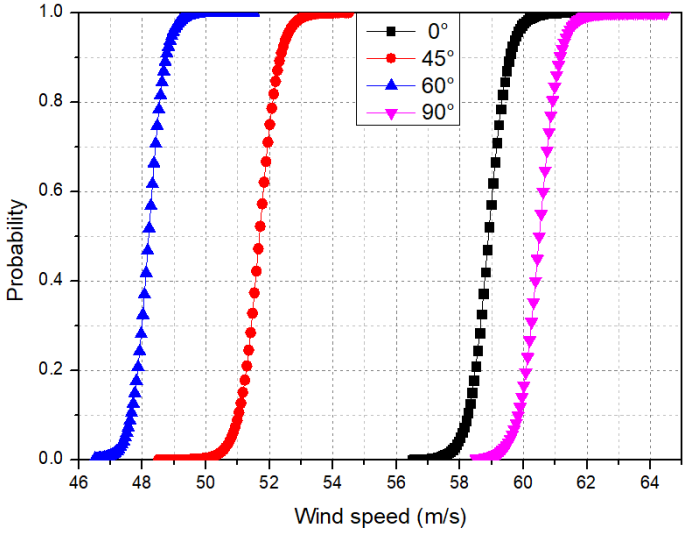

Figure 22. Fragility curve of collapse state under downburst.

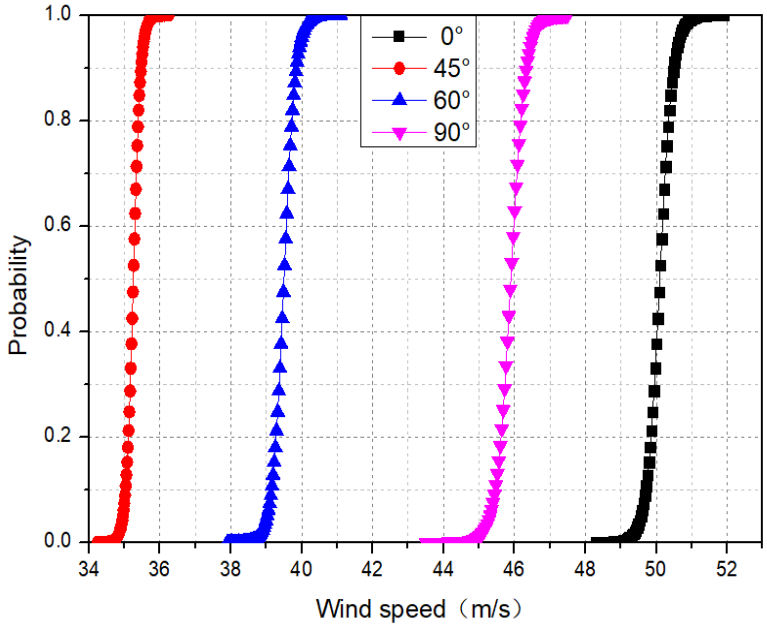

Figure 23. Fragility curve of collapse state of 35 KV transmission tower under ABL wind.

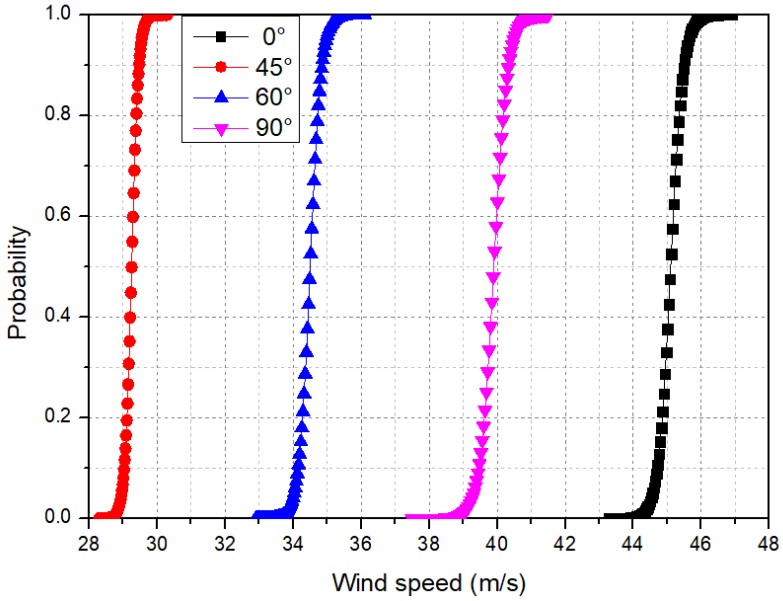

Figure 24. Fragility curve of collapse state under downburst.

3.6. Failure Probability Analysis

3.6.1. Evaluation Framework Based on Fragility Analysis

The downburst footprint is approximately a rectangle with length l_V and width w_V and area a_V [50]. The direction of the long axis of the footprint can be described by θ_V, with a size between π and 2π, as shown in Figure 25. The impact of the downburst on a transmission line is mainly concentrated in the area where the wind speed exceeds V. It is assumed that the annual average occurrence rate of downburst footprint with specific parameter (V,l_V,w_V,θ_v) in area A is $\tau(V\theta_v)$. The rate of intersection between a point in the area and downburst footprint in one year is:

$$v_{l,w,v,\theta_v} = \frac{l_V w_V \tau(V\theta_v)}{A} \tag{17}$$

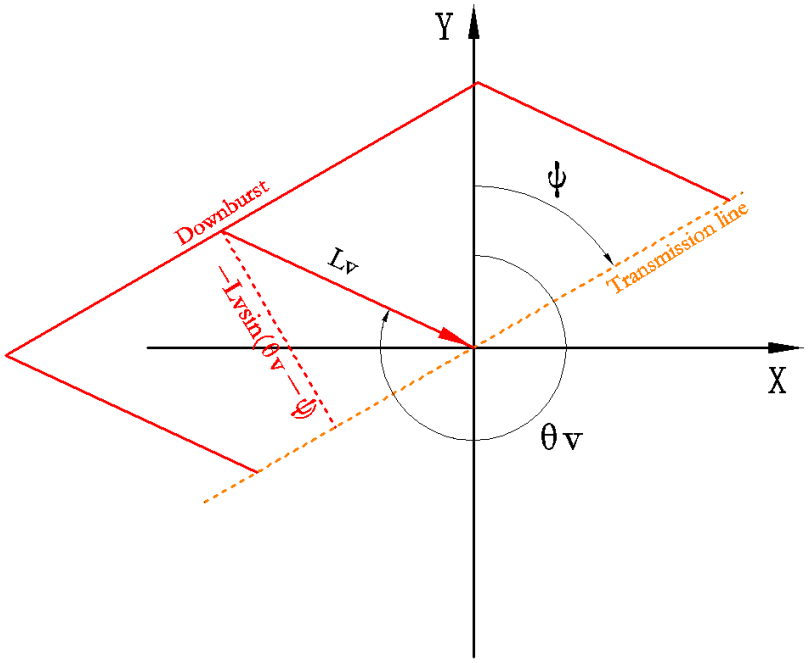

Figure 25. Oblique intersection of transmission line with downburst footprint.

Suppose a transmission line with a length of L is arranged in area A, and the line with orientation ψ lies between 0 and π. The directional probability $Pr(\theta_v)$ of downburst wind is considered. The rate of intersection per year between the transmission line and downburst footprints in area A is given as follows:

1. Normal to the transmission line

$$n_{l,w,v,\theta_v} = \frac{\tau(V\theta_v) l_V L Pr(\theta_v)}{A} = \frac{v_{l,w,v,\theta_v} L Pr(\theta_v)}{w_V} \tag{18}$$

2. Oblique to the transmission line

$$n_{l,w,v,\theta_v} = \frac{\tau(V\theta_v) l_V L |\sin(\theta_v - \psi)| Pr(\theta_v)}{A} = \frac{v_{l,w,v,\theta_v} L |\sin(\theta_v - \psi)| Pr(\theta_v)}{w_V} \tag{19}$$

3. Parallel to the transmission line

$$n_{l,w,v,\theta_v} = \frac{\tau(V\theta_v)(l_V + L) w_v Pr(\theta_v)}{A} = (1 + \frac{L}{l_V}) v_{l,w,v,\theta_v} Pr(\theta_v) \tag{20}$$

It is assumed that the occurrences of intersections with wind speeds exceeding V obey the Poisson distribution, and the probability of no intersections in any one year is equivalent to the cumulative distribution of the annual maximum wind speed in such events. It can be expressed as:

$$1 - P_{w\theta_v}(v > V) = \exp(-v_{w,v,\theta_v}) \cong 1 - v_{w,v,\theta_v} \tag{21}$$

Hence

$$P_{w\theta_v}(v > V) = v_{w,v,\theta_v} \tag{22}$$

The same method applies to the intersections with a transmission line:

$$1 - P_{w\theta_v}(a_V \cap L) = \exp(-n_{w,v,\theta_v}) \cong 1 - n_{w,v,\theta_v} \tag{23}$$

Hence

$$P_{w\theta_v}(a_V \cap L) = n_{w,v,\theta_v} \tag{24}$$

where $P_{w\theta_v}(v > V)$ represents the probability that the annual maximum wind speed from downburst footprints with characteristics w_V and θ_V, and having any l_V, intersecting a point in area A exceeds V. Correspondingly, $P_{w\theta_v}(a_V \cap L)$ represents the probability that the annual maximum wind speed from downburst footprints intersecting the transmission line exceeds V.

Accordingly, the intersection rate between the downburst footprint and the transmission line under each condition is:

1. Normal to the transmission line

$$P_{w\theta_v}(a_V \cap L) = P_{w\theta_v}(v > V)\frac{L}{w_v}Pr(\theta_v) \tag{25}$$

2. Oblique to the transmission line

$$P_{w\theta_v}(a_V \cap L) = P_{w\theta_v}(v > V)\frac{L}{w_v}|\sin(\theta_v - \psi)|Pr(\theta_v) \tag{26}$$

3. Parallel to the transmission line

$$P_{w\theta_v}(a_V \cap L) = \tau(V\theta_v)(l_V + L)\frac{w_v}{A} = (1 + \frac{L}{l_V})P_{w\theta_v}(v > V)Pr(\theta_v) \tag{27}$$

As for the width of the downburst footprint, Equations (25)–(27) show that a decrease in w_V is associated with an increase in the rate of intersection n_{l,w,v,θ_v}. If the width is less than the span, the action range of the downburst may only on one tower or none at all. Therefore, it can be assumed that the width of the downburst footprint is the transmission line span. For the case that the downburst footprint is parallel to the transmission line, according to the fragility curve calculated above, it can be known that the critical collapse wind speed in the 0° direction is about 30 m/s, and the downburst footprint length of Andrews air force base is about 5.5 km. The length of the downburst footprint under different direction angles can be obtained [34].

3.6.2. Case Study

There is a 10 km long north-south 220 KV transmission line in southeast Queensland, Australia. Tables 10 and 11 outline the return period R_V and directional probabilities $Pr(\theta_v)$ of downburst wind gusts for the region, respectively. Based on the given downburst wind speed and direction data, the transmission line layout conditions of 22.5°, 67.5°, 112.5°, and 157.5° are considered in this paper, as shown in Figure 26.

According to the above method, the probability of a downburst attacking the transmission line can be calculated. Combined with the fragility curve of 220 KV transmission tower in the collapse state under the downburst, the probability of transmission tower collapse caused by the downburst attacking the transmission line in different directions can be obtained. By adjusting the layout direction of transmission lines, the collapse probability of transmission towers under different layout conditions, different directions, and different wind speeds can be obtained, as shown in Figure 27. The favorable and unfavorable layout conditions for different directions are shown in Table 12.

Under the condition of different layouts of the transmission line and the same direction angle, the failure probability for a direction angle in the interval 2–6 is the largest and that in the interval 3–7 is the smallest, indicating that the wind directional probability has a great impact on the failure probability.

Table 10. Return periods for downburst wind gusts.

Wind Gust Speed (m/s)	Return Period (Years)	Wind Gust Speed (m/s)	Return Period (Years)
35	10.3	48	100
36	11.8	49	126
37	13.5	50	162
38	15.7	51	212
39	18.2	52	281
40	21.3	53	381
41	25.1	54	526
42	29.8	55	747
43	35.7	56	1090
44	43	57	1650
45	52	58	2600
46	64	59	4300
47	79	60	7700

Return period = 1/(annual probability of exceedance).

Table 11. Directional probabilities for downburst wind gusts.

$\mathbf{Pr}(\theta_{v1})$ θ_{v1}=22.5° Interval 2–6	$\mathbf{Pr}(\theta_{v2})$ θ_{v2}=67.5° Interval 1–5	$\mathbf{Pr}(\theta_{v3})$ θ_{v3}=112.5° Interval 4–8	$\mathbf{Pr}(\theta_{v4})$ θ_{v4}=157.5° Interval 3–7
0.343	0.293	0.192	0.172

Note: the downburst gusts in the direction of 22.5° are added to the downburst gust in the direction of 202.5°, etc.

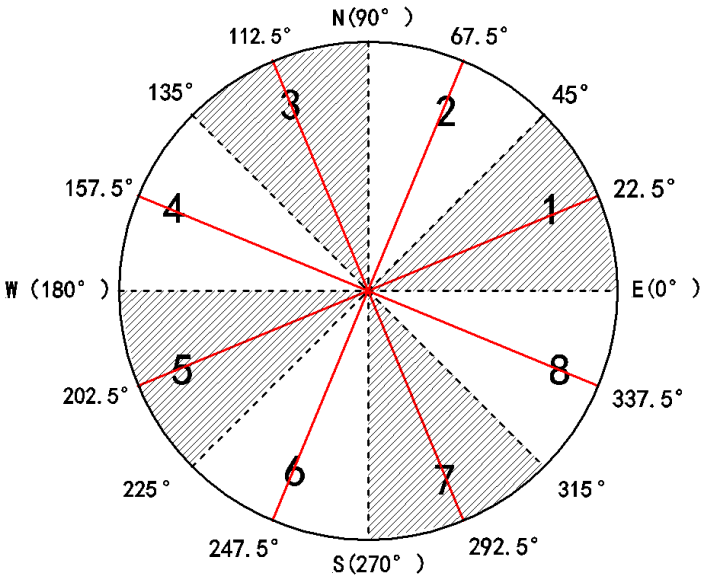

Figure 26. Transmission line layout conditions.

Table 12. Favorable and unfavorable layout conditions for different directions.

Layout Conditions	Direction Angle			
	0°/180°	45°/225°	90°/270°	135°/315°
Most favorable layout conditions	112.5°	67.5°	22.5°	157.5°
Most unfavorable layout conditions	67.5°	22.5°	157.5°	112.5°

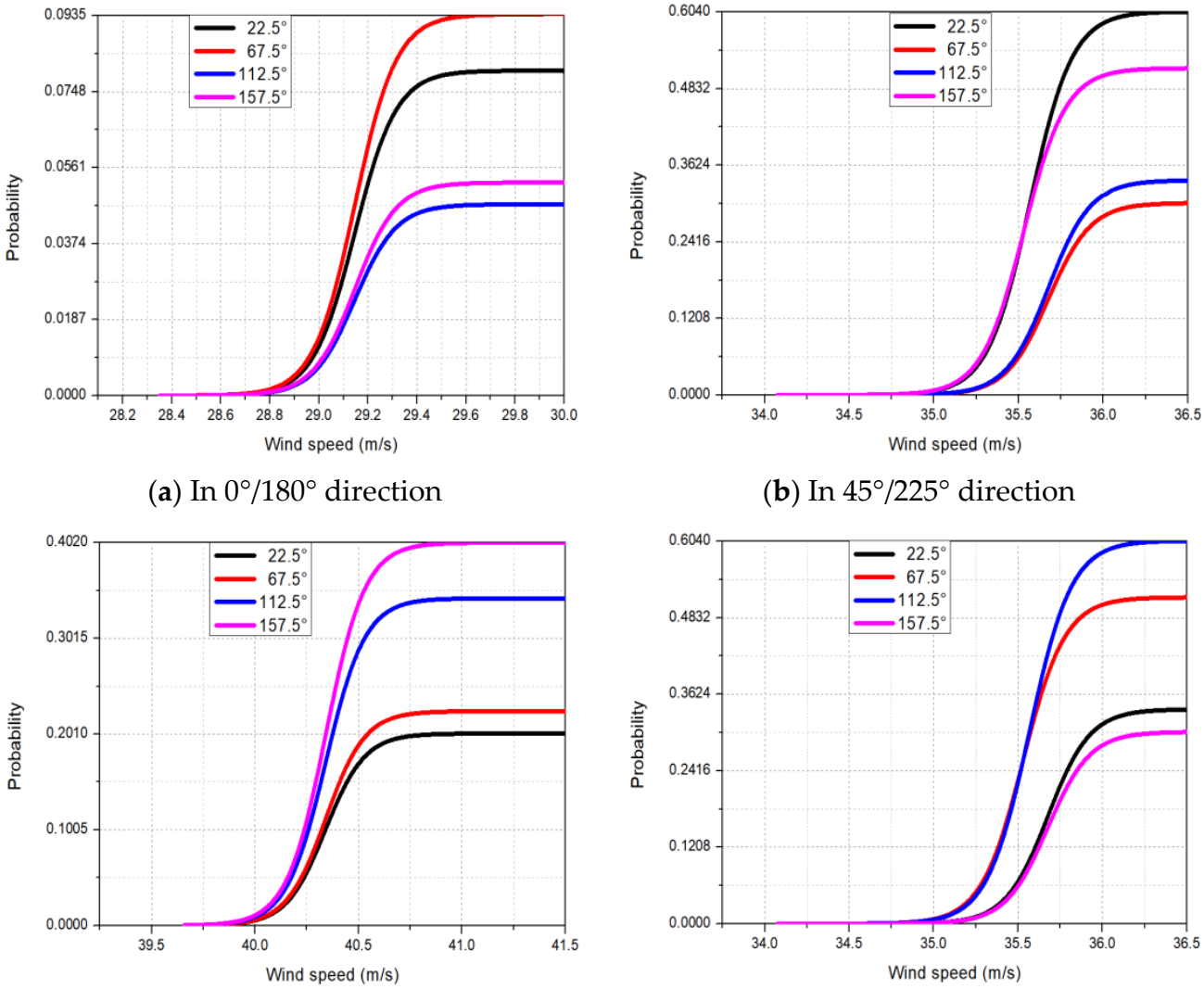

(**a**) In 0°/180° direction

(**b**) In 45°/225° direction

(**c**) In 90°/270° direction

(**d**) In 135°/315° direction

Figure 27. The probability of transmission tower collapse caused by a downburst attacking the transmission line in different directions.

According to the return period of downburst wind gusts, with the increase in wind speed, the return period becomes larger and larger, and the probability of a downburst attacking the transmission line becomes smaller and smaller. Figure 27 reflects the failure probability of the tower under the previous wind speed, and Figure 28 shows the failure probability of the tower under the full wind speed.

According to the above failure probability results, the average failure probability of four layout conditions is calculated under different wind speeds, and the average fragility curve of the transmission tower under different basic wind speeds is drawn, as shown in Figure 29. The results show that the most favorable arrangement is 157.5°, and the most unfavorable arrangement is 112.5°.

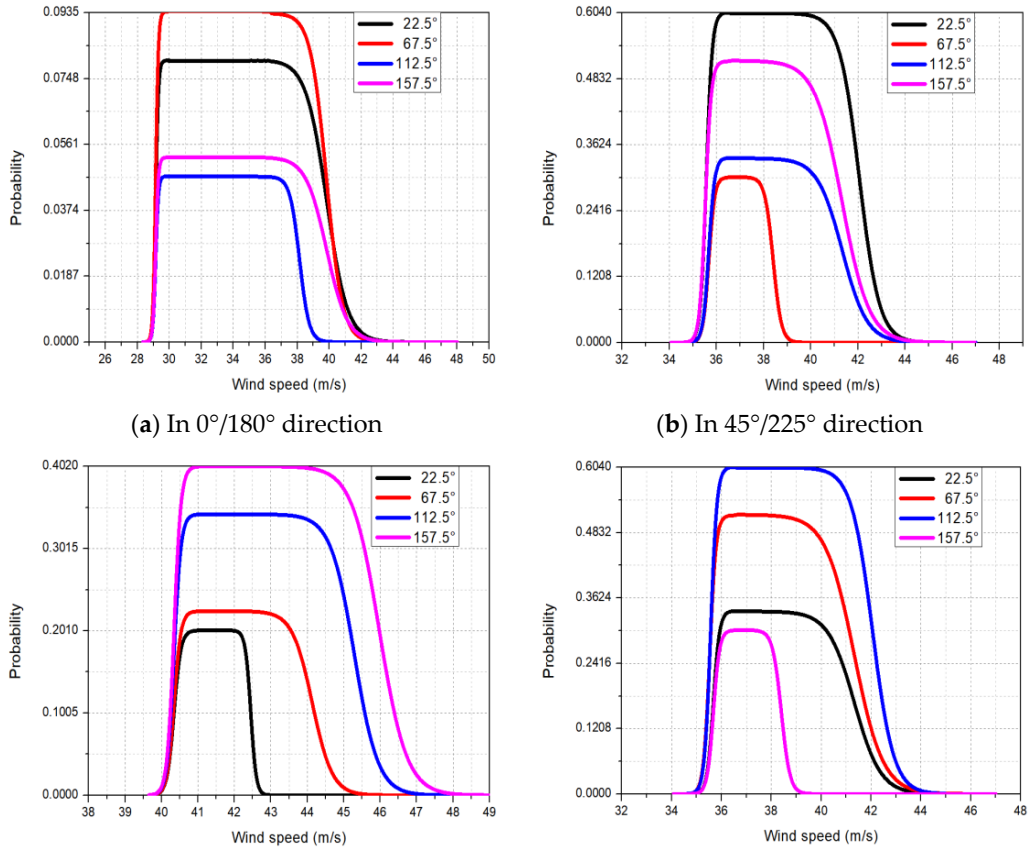

(**a**) In 0°/180° direction (**b**) In 45°/225° direction

(**c**) In 90°/270° direction (**d**) In 135°/315° direction

Figure 28. Failure probability of transmission tower under full wind speed.

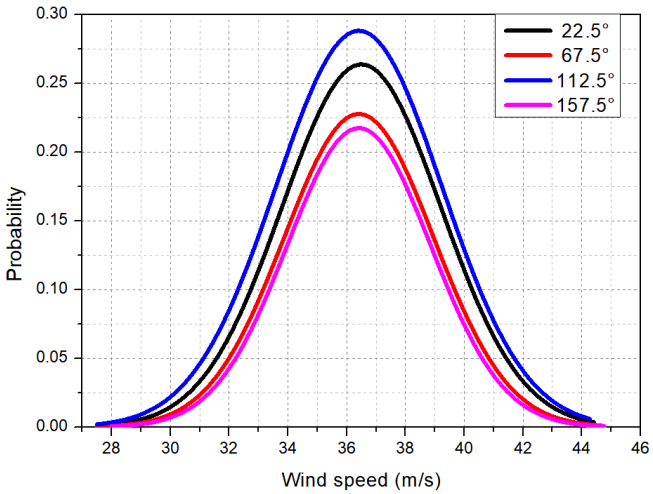

Figure 29. Average fragility curve of transmission tower under different basic wind speeds.

4. Summary and Conclusions

A novel framework for the fragility analysis of the transmission tower under the downburst is proposed. The framework will improve the wind-resistance design and wind-disaster prediction of the transmission tower. The wind-induced fragility of three types of transmission towers is analyzed under the effects of a downburst. Fragility analysis results of the transmission tower will vary with tower height and tower type. The main contents of this paper are as follows. The fragility curves of the transmission tower under the downburst and the ABL wind are compared considering the uncertainty

of resistance and the randomness of wind load effect, and the uncertain collapse of the transmission tower under the downburst is carried out. The position and corresponding probabilities of the initial buckling members of the transmission tower under the downburst are determined. Combined with the probability of wind speed and direction data of a region, the failure probability of the downburst attacking the transmission line causing the collapse of the transmission tower at different directions is calculated, and the optimal layout of transmission towers under a given wind field is studied. The innovation points and specific contributions of the current study are given as follows:

(1) The most unfavorable radial distance from the center of the downburst to the tower, as well as the most unfavorable wind attack angles, is analyzed by the parameter analysis of the fragility curves of the tower. It can be concluded that the location where the maximum response occurs is $R = 1.6D$, and the range of radial distance for slight damage status is wider than that for severe damage in all direction angles—the range far greater than the radial distance of collapse—because during the attacking process, with the increase in the radial distance, the time-varying mean wind speed of the downburst increases first and then decreases.

(2) Because almost half of the wind load on the tower comes from large-span transmission lines, the wind load effect on the tower varies significantly in different wind directions. On the other hand, the ultimate wind resistance capacity of the tower is also different depending on wind attack angles. Both of the reasons lead to the significant variation in the fragility curves at different angles.

(3) Uncertain collapse of the transmission tower under the downburst is carried out by nonlinear buckling analysis to indicate the failure mode and the most vulnerable main members. It provides some guidance for the maintenance and retrofit of the transmission tower under downburst wind load. It can be found that most of the initial buckling members are located near the first section of the transmission tower. The initial failure member is the main member, indicating that the main failure mode of the transmission tower belongs to bending failure. The main member is a compression bending component, which is the main component of the wind resistance of the transmission tower, while the diagonal member is an axial compression component, which is an auxiliary component of the wind resistance of the transmission tower. The instability of the diagonal member will not cause the collapse of the tower structure but will significantly decrease the stability of the main member.

(4) The fragility curves of the tower under the downburst are more dangerous than those under the ABL wind with the attack angle increasing from 0° to 90°. Compared with the ABL wind, the downburst, characterized by localization and high intensity, can often greatly exceed the ABL wind and cause the collapse of the transmission tower. In addition, the maximum average wind speed of the downburst first increases along the height, then decreases rapidly, and the maximum value occurs within the height range of the transmission tower structure.

(5) The probability of the downburst attacking the transmission line is related to the return period of wind speed, probabilities of attacking direction of a downburst, and the span of the transmission line. Based on the previous fragility analysis, considering the probability model of intensity and direction of the downburst, the collapse probability of the transmission tower caused by a downburst is obtained. By probability analysis of the parameters including layout conditions, different directions, and different wind speeds, it is found that the most favorable arrangement is 157.5°, and the most unfavorable arrangement is 112.5°.

Author Contributions: Conceptualization, C.Z.; methodology, C.Z. and D.W.; software, C.Z.; validation, C.Z.; formal analysis, G.H. and S.L.; investigation, Q.Y.; resources, G.H. and S.L.; data curation, C.Z.; writing—original draft preparation, C.Z.; writing—review and editing, Q.Y.; visualization, D.W.; supervision, D.W.; project administration, G.H. and S.L.; funding acquisition, D.W. All authors have read and agreed to the published version of the manuscript.

Funding: This research was funded by the National Natural Science Foundation of China (Grant Nos. 51878041, 51808078, 52108475 and 51908074) and 111 Project (Grant No. B18062).

Institutional Review Board Statement: Not applicable.

Informed Consent Statement: Not applicable.

Data Availability Statement: Not applicable.

Acknowledgments: The supports by the National Natural Science Foundation of China (Grant Nos. 51878041, 51808078, 52108475 and 51908074) and 111 Project (Grant No. B18062) are greatly acknowledged.

Conflicts of Interest: The authors declare no conflict of interest.

References

1. Fujita, T.T. Manual of downburst identification for project NIMROD. *Smrp*, 1978.
2. Fujita, T.T. Downbursts: Meteorological features and wind field characteristics. *J. Wind. Eng. Ind. Aerodyn.* **1990**, *36*, 75–86. [CrossRef]
3. Letchford, C.W.; Mans, C.; Chay, M.T. Thunderstorms—Their importance in wind engineering—A case for the next generation wind tunnel. *J. Wind. Eng. Ind. Aerodyn.* **2002**, *90*, 1415–1433. [CrossRef]
4. Sengupta, A.; Sarkar, P.P. Experimental measurement and numerical simulation of an impinging jet with application to thunderstorm microburst winds. *J. Wind. Eng. Ind. Aerodyn.* **2008**, *96*, 345–365. [CrossRef]
5. Wang, J.W. Failure Characteristics of Transmission Towers Subjected to Downbursts. In *Applied Mechanics and Materials*; Trans Tech Publications Ltd.: Stafa-Zurich, Switzerland, 2012; Volume 226, pp. 1161–1164.
6. Dempsey, D.; White, H.B. Winds wreak havoc on lines. *Transm. Distrib. World* **1996**, *48*, 32–37.
7. Xie, Q.; Zhang, Y.; Li, J. Investigation on tower collapses of 500kV Renshang 5237 transmission line caused by a downburst. *Power Syst. Technol.* **2006**, *30*, 59.
8. Wang, C.; Lou, W.J.; Li, H.N. Wind-induced dynamic response of high-rise transmission tower under downburst wind load. *J. ZheJiang Univ. Eng. Sci.* **2009**, *43*, 1520–1525.
9. Qu, W.L.; Liang, Z.P.; Wang, L.Z. Downburst's characteristics and its effect on wind-induced collapse of transmission tower. *J. Earthq. Eng. Eng. Vib.* **2010**, *30*, 120–126.
10. Fu, X.; Li, H.N.; Tian, L.; Wang, J.; Cheng, H. Fragility analysis of transmission line subjected to wind loading. *J. Perform. Constr. Facil.* **2019**, *33*, 04019044. [CrossRef]
11. Cai, Y.; Xie, Q.; Xue, S.; Hu, L.; Kareem, A. Fragility modelling framework for transmission line towers under winds. *Eng. Struct.* **2019**, *191*, 686–697. [CrossRef]
12. Fu, X.; Li, H.N.; Li, G.; Dong, Z.Q. Fragility analysis of a transmission tower under combined wind and rain loads. *J. Wind. Eng. Ind. Aerodyn.* **2020**, *199*, 104098. [CrossRef]
13. Tian, L.; Zhang, X.; Fu, X. Fragility analysis of a long-span transmission tower–line system under wind loads. *Adv. Struct. Eng.* **2020**, *23*, 2110–2120. [CrossRef]
14. Ma, L.; Khazaali, M.; Bocchini, P. Component-based fragility analysis of transmission towers subjected to hurricane wind load. *Eng. Struct.* **2021**, *242*, 112586. [CrossRef]
15. Wang, D.; Li, S.; Sun, C.; Huang, G.; Yang, Q. Assessment of wind-induced fragility of transmission towers under quasi-static wind load. *Wind. Struct.* **2021**, *33*, 343–352.
16. Dikshit, S.; Alipour, A. A moment-matching method for fragility analysis of transmission towers under straight line winds. *Reliab. Eng. Syst. Saf.* **2023**, *236*, 109241. [CrossRef]
17. Savory, E.; Parke, G.A.; Zeinoddini, M.; Toy, N.; Disney, P. Modelling of tornado and microburst-induced wind loading and failure of a lattice transmission tower. *Eng. Struct.* **2001**, *23*, 365–375. [CrossRef]
18. Hoxey, R.; Robertson, A.; Toy, N.; Parke GA, R.; Disney, P. Design of an experimental arrangement to study the wind loads on transmission towers due to downbursts. *WIT Trans. Built Environ.* **2003**, *71*, 395–404.
19. Chen, L.; Letchford, C.W. A deterministic–stochastic hybrid model of downbursts and its impact on a cantilevered structure. *Eng. Struct.* **2004**, *26*, 619–629. [CrossRef]
20. Chay, M.T.; Albermani, F.G.; Hawes, H. Wind loads on transmission line structures in simulated downbursts. In *First World Congress on Asset Management*; IEEE: Gold Coast, Australia, 2006; pp. 1–13.
21. Shehata, A.Y.; El Damatty, A.A. Behaviour of guyed transmission line structures under downburst wind loading. *Wind. Struct.* **2007**, *10*, 249–268. [CrossRef]
22. Aboshosha, H.; El Damatty, A.A. Capacity of electrical transmission towers under downburst loading. In Proceedings of the First Australasia and South-East Asia Structural Engineering and Construction Conference, Perth, Australia, 28 November–2 December 2012.
23. Yang, S.C.; Hong, H.P. Nonlinear inelastic responses of transmission tower-line system under downburst wind. *Eng. Struct.* **2016**, *123*, 490–500. [CrossRef]

24. Wang, F.Y.; Xu, Y.L.; Qu, W.L. Multi-scale failure analysis of transmission towers under downburst loading. *Int. J. Struct. Stab. Dyn.* **2018**, *18*, 1850029. [CrossRef]
25. Zheng, H.D.; Fan, J. Progressive collapse analysis of a truss transmission tower-line system subjected to downburst loading. *J. Constr. Steel Res.* **2022**, *188*, 107044. [CrossRef]
26. Mara, T.G.; Hong, H.P.; Lee, C.S.; Ho, T.C.E. Capacity of a transmission tower under downburst wind loading. *Wind. Struct.* **2016**, *22*, 65–87. [CrossRef]
27. El Damatty, A.; Elawady, A. Critical load cases for lattice transmission line structures subjected to downbursts: Economic implications for design of transmission lines. *Eng. Struct.* **2018**, *159*, 213–226. [CrossRef]
28. Elawady, A.; Aboshosha, H.; El Damatty, A. Aero-elastic response of transmission line system subjected to downburst wind: Validation of numerical model using experimental data. *Wind. Struct.* **2018**, *27*, 71–88.
29. Ibrahim, I.; El Damatty, A.; Elawady, A. The Dynamic Effect of Downburst Winds on the Longitudinal Forces Applied to Transmission Towers. *Front. Built Environ.* **2019**, *5*, 59. [CrossRef]
30. Fang, Z.; Wang, Z.; Zhu, R.; Huang, H. Study on wind-induced response of transmission tower-line system under downburst wind. *Buildings* **2022**, *12*, 891. [CrossRef]
31. Zhong, Y.; Li, S.; Yan, Z.; Liu, X.; Luo, J.; Jin, W. Study on Stability of Transmission Tower-Line System under a Downburst. *Buildings* **2022**, *12*, 1338. [CrossRef]
32. Biondini, F.; Frangopol, D.M. Life-cycle performance of deteriorating structural systems under uncertainty. *J. Struct. Eng.* **2016**, *142*, F4016001. [CrossRef]
33. Fu, X.; Li, H.N. Uncertainty analysis of the strength capacity and failure path for a transmission tower under a wind load. *J. Wind. Eng. Ind. Aerodyn.* **2018**, *173*, 147–155. [CrossRef]
34. Holmes, J.D.; Oliver, S.E. An empirical model of a downburst. *Eng. Struct.* **2000**, *22*, 1167–1172. [CrossRef]
35. Oseguera, R.M.; Bowles, R.L. *A Simple, Analytic 3-Dimensional Downburst Model Based on Boundary Layer Stagnation Flow*; NASA Technical Memorandum No. 100632; NASA: Washington, DC, USA, 1988.
36. Wood, G.S.; Kwok, K.C.; Motteram, N.A.; Fletcher, D.F. Physical and numerical modelling of thunderstorm downbursts. *J. Wind. Eng. Ind. Aerodyn.* **2001**, *89*, 535–552. [CrossRef]
37. Vicroy, D.D. Assessment of microburst models for downdraft estimation. *J. Aircr.* **1992**, *29*, 1043–1048. [CrossRef]
38. Li, J.H.; Wu, C.P.; Chen, S.S. Simulation of non-stationary fluctuating wind velocity in downburst. *J. Vib. Shock.* **2014**, *33*, 54–60.
39. Shinozuka, M.; Deodatis, G. Simulation of multi-dimensional Gaussian stochastic fields by spectral representation. *Appl. Mech. Rev.* **1996**, *49*, 29–53. [CrossRef]
40. Peng, L.; Huang, G.; Chen, X.; Kareem, A. Simulation of multivariate nonstationary random processes: Hybrid stochastic wave and proper orthogonal decomposition approach. *J. Eng. Mech.* **2017**, *143*, 04017064. [CrossRef]
41. DL/T5154-2012; *Technical Code for the Design of Tower and Pole Structures of Overhead Transmission Lines*; China Planning Press: Beijing, China, 2012.
42. Aboshosha, H.; El Damatty, A. Dynamic response of transmission line conductors under downburst and synoptic winds. *Wind. Struct.* **2015**, *21*, 241–272. [CrossRef]
43. Xu, L.; Xing, F.; Kai, X.; Jia, W.; Ming, N.; Li, H.N.; Xie, W.P. Failure Analysis of a Transmission Tower Subjected to Wind Load Using Uncertainty Method. *Proc. CSEE* **2018**, *38*, 266–274. (In Chinese)
44. Huang, B.C.; Wang, C.J. *The Wind Resistance Analysis Principle and Application in Structures*; Tongji University Press: Shanghai, China, 2008; pp. 29–30. (In Chinese)
45. Shinozuka, M.; Deodatis, G. Simulation of stochastic processes by spectral representation. *Appl. Mech. Rev.* **1991**, *44*, 191–204. [CrossRef]
46. Zhao, N.; Huang, G. Wind velocity field simulation based on enhanced closed-form solution of Cholesky decomposition. *J. Eng. Mech.* **2020**, *146*, 04019128. [CrossRef]
47. Deng, H.Z.; Xu, H.J.; Duan, C.Y.; Jin, X.H.; Wang, Z.H. Experimental and numerical study on the responses of a transmission tower to skew incident winds. *J. Wind. Eng. Ind. Aerodyn.* **2016**, *157*, 171–188. [CrossRef]
48. Yang, F.; Yang, J.; Niu, H.; Zhang, H. Design wind loads for tubular-angle steel cross-arms of transmission towers under skewed wind loading. *J. Wind. Eng. Ind. Aerodyn.* **2015**, *140*, 10–18. [CrossRef]
49. Yang, F.; Dang, H.; Niu, H.; Zhang, H.; Zhu, B. Wind tunnel tests on wind loads acting on an angled steel triangular transmission tower. *J. Wind. Eng. Ind. Aerodyn.* **2016**, *156*, 93–103. [CrossRef]
50. Oliver, S.E.; Moriarty, W.W.; Holmes, J.D. A risk model for design of transmission line systems against thunderstorm down burst winds. *Eng. Struct.* **2000**, *22*, 1173–1179. [CrossRef]